

JAERI-Research
99-063



JP0050012



**ANALYSIS OF INTERNAL TRANSPORT BARRIER HEAT
DIFFUSIVITY FROM HEAT PULSE PROPAGATION
CREATED BY ABRUPT VARIATION OF DIFFUSIVITY
IN JT-60U REVERSE SHEAR PLASMAS**

November 1999

**Sergei V. NEUDATCHIN*, Tomonori TAKIZUKA,
Hiroshi SHIRAI, Takaaki FUJITA, Akihiko ISAYAMA,
Yoshihiko KOIDE and Yutaka KAMADA**

**日本原子力研究所
Japan Atomic Energy Research Institute**

本レポートは、日本原子力研究所が不定期に公刊している研究報告書です。
入手の間合わせは、日本原子力研究所研究情報部研究情報課（〒319-1195 茨城県那珂郡東海村）あて、お申し越してください。なお、このほかに財団法人原子力弘済会資料センター（〒319-1195 茨城県那珂郡東海村日本原子力研究所内）で複写による実費頒布をおこなっております。

This report is issued irregularly.
Inquiries about availability of the reports should be addressed to Research Information Division, Department of Intellectual Resources, Japan Atomic Energy Research Institute, Tokai-mura, Naka-gun, Ibaraki-ken, 319-1195, Japan.

© Japan Atomic Energy Research Institute, 1999

編集兼発行 日本原子力研究所

Analysis of Internal Transport Barrier Heat Diffusivity from
Heat Pulse Propagation Created by Abrupt Variation of Diffusivity
in JT-60U Reverse Shear Plasmas

Sergei V. NEUDATCHIN*, Tomonori TAKIZUKA, Hiroshi SHIRAI, Takaaki FUJITA,
Akihiko ISAYAMA, Yoshihiko KOIDE and Yutaka KAMADA

Department of Fusion Plasma Research
Naka Fusion Research Establishment
Japan Atomic Energy Research Institute
Naka-machi, Naka-gun, Ibaraki-ken

(Received October 28, 1999)

A new source of Heat Pulse Propagation (HPP) is found in JT-60U RS plasmas. HPP is created by abrupt in time and wide in space variation of heat diffusivity ("event"). Events are seen as the simultaneous rise and decay of electron temperature T_e on two zones. For the event described in present paper, the region of strong T_e rise (~ 20 keV/s) is well localized (~ 4 cm) in space initially. Later in time, a slow diffusive broadening of the rising T_e perturbation is seen throughout ITB region. The HPP is analyzed analytically and numerically. Values of the electron heat diffusivity as low as $\sim 0.1 \text{ m}^2/\text{s}$ are found in the region with ~ 8 cm width fully located in positive shear space zone. A similar low value of the ion heat diffusivity is obtained for ion HPP. An important consequence of HPP analysis is an absence of electron and ion "heat pinch" in the ITB region.

Keywords: Tokamak, JT-60U, Reverse Shear, Internal Transport Barrier, Heat Diffusivity,
Heat Pulse Propagation, Transport Analysis

* Nuclear Fusion Institute, Russian Research Center "Kurchatov Institute", Moscow, Russia

拡散係数の急激変動が誘起する熱パルス伝搬に基づく
JT-60U 負磁気シアプラズマ中の内部輸送障壁熱拡散係数の解析

日本原子力研究所那珂研究所炉心プラズマ研究部
Sergei V. NEUDATCHIN*・滝塚 知典・白井 浩・藤田 隆明
諫山 明彦・小出 芳彦・鎌田 裕

(1999年10月28日受理)

JT-60U 中の負磁気シアプラズマにおいて、熱パルス伝搬の新しい発生源を発見した。熱拡散係数の時間的に急激で空間的に幅広い変動（"事象"）が熱パルス伝搬を引き起こす。この"事象"においては、電子温度の上昇する領域と下降する領域の2領域が同時に観測される。現論文に記述される事象では、非常に急激な電子温度上昇（ $\sim 20 \text{ keV/s}$ ）が局所的（ $\sim 4 \text{ cm}$ ）に発生する。その後時間が進むに従って、上昇した温度の変動が内部輸送障壁領域をゆっくりと拡散的に広がっていく。この熱パルス伝搬を解析的・数值的に研究した。約 8 cm 幅の領域において、電子の熱拡散係数は、約 $0.1 \text{ m}^2/\text{s}$ という小さな値になっていることが分かった。この領域は磁気シアが正になっているところまで含んでいる。イオンの熱パルス伝搬も解析し、イオン熱拡散係数も電子と同様な低い値となっていることを示した。さらにこの熱パルス伝搬解析から、内部輸送障壁領域中には、電子もイオンもともに"熱ピンチ"は存在しないことを明らかにした。

Contents

1. Introduction	1
2. ITB Evolution after Strong ITB Formation in Pulse E32423	5
2.1 Abrupt Variations of Heat Diffusivity after Strong ITB Formation	6
2.2 Comparison of T_e and T_i Space-time Evolution	9
2.3 Experimental Picture of Heat Pulse Propagation	10
3. Analysis of HPP	10
3.1 Analytical Analysis of HPP	11
3.2 Numerical Analysis of HPP	13
4. Consequences for Heat Flux Structure	18
5. Discussion	21
6. Summary	24
Acknowledgments	25
References	26

目 次

1. はじめに	1
2. パルス E32423 における強い ITB 形成後の ITB の発展	5
2.1 強い ITB 形成後の熱拡散係数の急激な変動	6
2.2 T_e と T_i の時間的空間的発展の比較	9
2.3 熱パルス伝搬 (HPP) の実験的描像	10
3. HPP の解析	10
3.1 HPP の解析的研究	11
3.2 HPP の数値的解析	13
4. 熱束構造の結果	18
5. 考察	21
6. まとめ	24
謝辞	25
参考文献	26

This is a blank page.

1. Introduction

An understanding and controlling of ITB properties are one of the mostly important issues of today's tokamaks fusion program. The record value of the DT-equivalent fusion-power-amplification factor $Q_{DT}^{eq}=1.25$ was achieved recently in RS discharges with ITB in JT-60U [1]. Significant progress is seen in the development of the Steady State RS (SSRS) scenario [1] and Steady State high- β_p scenario [2] in JT-60U plasmas with ITB. The RS mode is considered to be one of the feasible modes for the steady-state and enhanced performance operation in ITER [3].

Key factors involved in the processes of the ITB evolution during RS and normal shear discharges have not been fully understood yet. A lot of experimental studies concerning this topic have been performed on JT-60U. Characteristics of the ITB for RS plasmas and high- β_p plasmas (with normal shear) were compared [4]. Two types of ITB, "parabolic" (or weak) and "box" (or strong) type, were observed and transport properties for these cases were analyzed [5]. Fast transient phenomena (events) were often observed in plasmas with ITB; sudden rise or decay of temperature near outer boundary of the strong ITB region in RS plasmas [6,7] and discontinuous in time improvements of the ITB properties in normal shear plasmas [7,8].

The events were studied in details recently [9,10]. It was shown that events are seen as an appearing of "bipolar" perturbation of T_e - the simultaneous rise and decay of T_e on two zones separated by the region without variation of T_e (located near the minimum of q profile q_{min} in many cases). Events are the common intrinsic feature of the various JT-60U RS pulses with strong ITB, with weak ITB and without ITB. T_e variation after event is strictly created by abrupt (within few ms) χ_e variation at time of event. Spatial region of χ_e reduction (or increase) is wide in space (sometimes around 0.3 of minor radius) and well extended to the zone of T_e decay (or rise). In many cases this spatial region spreads well to the positive shear space zone.

A major problem in clarifying the nature of local heat transport in tokamak plasmas is the lack of accurate direct measurements of the local heat fluxes. Usually these fluxes are obtained from detailed power balance calculations. However, it is not easy to separate electron and ion heat fluxes from the total flux, especially in some of the high performance regimes. Moreover, even knowledge of heat diffusivities obtained from power balance $\chi_{e,i}^{PB}$, is not enough to fully resolve a structure of heat flux. The reason lies in old, not fully resolved question of existence of a “heat pinch” (or a large inward convective heat flux) in tokamak plasmas [11,12]. In this case $\chi_{e,i}^{PB}$ values are not real values of $\chi_{e,i}$, but are smaller values linked with difference (for nearly steady state conditions) between large outward and inward heat fluxes. The study of heat pulse propagation (HPP) is a powerful tool to obtain crucial information about heat flux structure. Many analytical and numerical methods for HPP studies were developed, in particular, for ECRH induced [13-16] and sawteeth induced HPP [16-20]. The way of HPP study development was not easy. Some of the results of sawteeth induced HPP study were strongly and unpredictably varied without any connection with plasma parameters variation. “Mystery” of sawteeth-induced HPP study was especially clearly seen in TFTR results [18], where values of χ_e^{HP} (described just below) obtained by time-to-peak method [17] were increased by 5-10 times during quasi-steady-state plasmas evolution seen just as a light amplification of sawteeth crashes. The question, arisen many times in discussions at conferences and workshops, was: “ *Is it possible with HPP study to obtain anything related to the heat transport ?* ”.

The value measured by HPP analysis is not χ_e^{PB} value but $\chi_e^{HP} = \delta\Gamma_e / (n_e \nabla \delta T_e)$ value, where χ_e^{HP} is dynamic electron heat diffusivity, $\delta\Gamma_e$ is the electron thermal flux perturbation, n_e is electron density and $\delta\nabla T_e$ is electron temperature gradient perturbation. For L-modes with central heating, χ_e^{HP} values are usually few times greater than χ_e^{PB} values [15,18] (so called

“enhanced HPP”). This difference can be explained by either a dependence of χ_e on ∇T_e [11,18], or by the presence of a large convective inward heat flux (so called “heat pinch”) [11,12]. A χ_e dependence on ∇T_e , however, does not affect the diffusive picture of HPP since we can write [11]: $\chi_e^{\text{HP}} = \chi_e^{\text{PB}} + (\partial \chi_e^{\text{PB}} / \partial \nabla T_e) \nabla T_e$. The study of outward enhanced HPP does not usually allow us to separate χ_e dependence on ∇T_e from presence of “heat pinch” [11].

A “mystery” of sawteeth induced HPP was resolved by creation of the new method [21-22] for HPP study by analyzing the decay of temperature perturbation induced by sawteeth. All previous methods for the sawteeth induced HPP study were based on numerical or analytical analysis of the outward HPP. This analysis of the decay is neither the study of pure outward nor inward HPP but in some sense the study of the spread of the initial perturbation in both directions simultaneously. One of the advantages of this method is automatical exclusion of so-called “ballistic” phase [23] of HPP from the analysis. “Ballistic” phase is seen as short-time scale (within one ms usually) and sometimes very wide (up to 0.9 of minor radius in low-q JET pulses [22]) spreading of the temperature perturbation after MHD-phase of a sawteeth crash. Previous results of sawteeth induced HPP study (especially on TFTR and JET due to powerful sawteeth in many regimes) were sometimes distorted in an unknown manner by the “ballistic” phase incorporated invisibly into the analysis.

Typical values of χ_e^{HP} are equal to few m^2/s near half of minor radius in on-axis heated L-mode plasmas [15,21,22]. The problem of “heat pinch” is not fully studied for these regimes. An absence of significant “heat pinch” was proved for some improved confinement regimes. Low values of χ_e^{HP} (near $0.7 \text{ m}^2/\text{s}$) were determined from sawteeth induced HPP in VH-mode JET regimes [21,22]. The upper limit of convective velocity was about 0.4 m/s . Slow inward HPP was observed during off-axis ECRH in L-mode on T-10 [24] and during off-axis ICRH in Pellet Enhanced Performance (PEP) L-mode on

JET [25]. Surprisingly low value of $\chi_e^{\text{HP}} = 0.14 \text{ m}^2/\text{s}$ was obtained on T-10 [26], when outward HPP was created by on-axis ECRH imposed on a broad steady state T_e profile created previously by off-axis ECRH. Two groups of gyrotrons with two different frequencies for simultaneous on- and off-axis heating were operated together during HPP. These experiments demonstrated the absence of significant inward convective electron heat fluxes during some of the good electron confinement regimes. However, the experimental data could be described by a complicated “canonical profile” model [27] in which the inward convective heat flux disappear with large deviations of the T_e profile from the “canonical” one. This model also gives reasonable agreement with some of the JT-60U RS discharges [28].

Traditional reasons of HPP are variations of heat sources or sinks or fast redistribution of temperature profile by sawteeth crash, pellet injection, etc. Inward HPP created by simultaneous temperature rise or decay in all volume located outside ~ 0.3 of minor radius due to “fast” L-H-L transitions was analyzed in [29]. Sudden simultaneous (within few ms) drops or rises (jumps) of χ in 90% of plasma volume are seen during “fast” L-H-L transitions observed in some regimes of JT-60U [30] and JET [21,29,31]. We can call this HPP as “transition induced HPP”. It is HPP from the boundary of the region covered by abrupt variation of χ to the not disturbed region.

By our up to date knowledge, HPP was not studied neither in ITB region nor in any region of RS plasmas anywhere in the world. Profiles of $\chi_{e,i}$ were obtained by transport codes calculations for nearly steady-states conditions. Transport properties of the ITB in positive shear zone were never analyzed in JT-60U RS discharges because no one example of quasi-steady-state plasmas with ITB formed in positive shear region is known.

Behaviors of T_e and T_i during ITB evolution after strong ITB formation in an RS pulse are presented in Section 2. Profiles of χ_e variations for two events are evaluated. Electron and ion outward HPP created by the last

event fully located in positive shear zone is described. It is HPP throughout ITB region with confinement abruptly improved by this event. Electron and ion HPP is analyzed analytically and numerically in Section 3. The way to obtain analytical method, originally created for ECRH-induced HPP [14], is also briefly described in Section 3 because it was never published in English. Consequences of HPP analysis for a heat flux structure inside ITB are highlighted in Section 4. A new interpretation of a very slow HPP measured in one unusual regime of T-10 is proposed in Section 5. Summary is the content of Section 6.

2. ITB evolution after strong ITB formation in pulse E32423

In the present paper we analyze the experimental result of an RS discharge E32423 in JT-60U in time interval from $t = 6.56$ to 6.67 s. Some results of this shot were reported in reference [32]. This shot was studied in more details recently [10]. Many events were found and three of them were described in terms of abrupt electron thermal diffusivity variations $\delta\chi_e$. Plasma parameters are the following; the major radius at the magnetic axis $R_0 = 3.3$ m, the minor radius $a = 0.86$ m, the elongation $\kappa = 1.45$ and the toroidal field at the magnetic axis $B_t = 3.8$ T. The plasma current I_p is increased to create the RS configuration and becomes constant $I_p = 1.5$ MA after $t = 5.6$ s. The plasma is heated by the NBI.

Waveforms of this discharge around our time interval of interest are shown in figure 1; the stored energy measured by diamagnetic loop W_{dia} , the injected NB power P_{NB} , the ion and electron temperatures T_i and T_e near $\rho = 0.5$, where ρ denotes the volume averaged minor radius normalized by the radius of a separatrix magnetic surface. The time of strong ITB formation is labeled by an arrow A. A profile of $\delta\chi_e(r)$ for this event A was obtained in reference [10]. Times of two another events are labeled by arrows B and C consequently.

Radial profiles of T_i given by the charge exchange recombination spectroscopy measurement (circles), T_e by the ECE Fourier transformed spectroscopy measurement (squares) and n_e by the YAG Thomson scattering measurement (triangles) just before $t = 6.560$ s (event A) are shown in figure 2. These profiles are determined in a magnetic configuration given by an equilibrium calculation with q profiles measured by MSE. The profile of q at $t = 6.72$ s is shown by dotted line in figure 2. The profiles of T_i for $t = 6.605$ s (before event C) and for $t = 6.67$ s (dashed and solid lines on figure 2) represents temperatures evolution with clear signs of ITB formation in outer region. ITB “foot” is still not well seen because the transient process of temperature evolution is not finished yet. In the present paper we mainly focus on the analysis of the T_i and T_e evolution after event C.

2.1 Abrupt variations of heat diffusivity after strong ITB formation

The ECE heterodyne radiometer with the 12 channels high space resolution (1.7cm half width for this pulse) [33] is used for detailed T_e measurements. Absolute calibration is done by using the data of Fourier ECE measurement just before the event, like it was done in references [9,10,32]. An evolution of T_e measured with radiometer is shown on Fig. 3. A variation of T_e after event A was described in details in reference [10]. It is seen as simultaneous rise of $T_{e\ 1-6}$ (T_e on channels 1-6) and decay of $T_{e\ 9-12}$. Spatial regions of T_e rise and decay are separated by the region without T_e variation (channels 7 and 8). Radial position of channel 7 is located near q_{min} . It is a typical picture for numerous events seen throughout various stages of ITB evolution in pulse 32423 [20] and in other RS pulses. A profile of $\delta\chi_e$ for the event A was obtained in reference [10] and is shown in Fig. 4 by dotted line.

Event B is seen as sudden simultaneous appearance of the negative values of $\delta \partial T_e / \partial t$ at and positive values of $\delta \partial T_e / \partial t$. An appearance of the discontinuous change of T_e is explained in reference [10] by the jump of χ_e in time across the event at $t = t_0$. It is changed abruptly at $t = t_0$ from χ_e to $\chi_e + \delta \chi_e$. The difference of transport equations between two phases is given as follows.

$$1.5 n_e \delta \partial T_e / \partial t = -\text{div} \{ n_e [\delta \chi_e \nabla T_e + (\chi_e + \delta \chi_e) \delta \nabla T_e] \} \quad (1)$$

An influence of possible perturbation of the density flux is estimated analytically and numerically in reference [10]. We regard this influence in the present study. In order to obtain the value of $\delta \chi_e$ from the measurement of $\delta \partial T_e / \partial t$, we integrate Equation (1) over volume. Because of the limited measurement accuracy, we use the time averaged values for $t_0 < t < t_0 + \Delta t$ instead of the instantaneous values just after $t = t_0$. In the present study an interval of $\Delta t = 10$ ms is adopted for the event B. The relation between $\delta \chi_e$ and $\delta \partial T_e / \partial t$ is expressed as

$$\begin{aligned} & \langle \delta \chi_e \rangle + \langle (\chi_e + \delta \chi_e) \delta \nabla T_e \rangle / \nabla T_e \\ & = 1.5 \left\{ \int_0^{V(r)} n_e \langle \delta \partial T_e / \partial t \rangle dV \right\} / \{ n_e \nabla T_e A(r) \} \end{aligned} \quad (2)$$

where brackets $\langle \rangle$ denote time averaged quantity, $A(r)$ is the surface area of a magnetic surface at a minor radius r , and $V(r)$ is the volume surrounded by this surface. The second term in the LHS of equation (2) originates from the diffusion spreading of the perturbed temperature δT_e , whose weight in equation (2) is small unless Δt is long.

The corresponding profile of positive $\delta\chi_e$ obtained for the event B with Equation (2) without second term in LHS is shown on Fig. 4 by solid line. We call event B - a “partial degradation” of ITB.

A spatial region covered by events sometimes is not located around position of q_{\min} . An event C is seen as strong rise of $T_{e\ 8,9}$ at ($\delta\partial T_e/\partial t \sim 20$ keV/s in first 10 ms after time C) and some small negative $\delta\partial T_e/\partial t$ at channels 11,12, i.e. event C is fully located in positive shear zone. We expect that negative values of $\delta\partial T_e/\partial t$ should be seen outside channel 12 also, but uncertainty of T_e behavior outside channel 12 is not important for our analysis. The spatial zone of T_e rise is very well localized in space. It is suggested in our analysis that the region of T_e rise is located between the left boundary of the half space resolution of channel 8 and the right one of channel 9 (~ 4 cm width). The corresponded profile of negative $\delta\chi_e$ obtained with Equation (2) is shown on Fig. 4 by broken line. The 5 ms time interval was adopted in this case because of faster thermal diffusivity created spreading of the initial δT_e in space due to small ~ 4 cm width of δT_e rise region.

We call event C “improvement of ITB” in positive shear zone. The strong rise of $T_{e\ 8,9}$ is created by heat flux “trapping” in the similarly space localized region of the inner edge of χ_e improvement (see Fig. 4). The total result of events B+C (or sum of on the $\delta\chi_e$ profiles created by events B and C) on $\delta\chi_e$ profile is a light degradation of the confinement inside position of q_{\min} and an improvement outside position of q_{\min} . It is a way of outward ITB motion.

Profiles of $\delta\chi_e$ obtained from Equation (2) are inversely proportional to ∇T_e values. As described in the beginning of Section 2.1, ∇T_e values are obtained from heterodyne absolute calibration against Fourier ECE measurements just before event A. The local structure of ∇T_e could be lost easily with such a calibration from low space resolution measurements.

2.2 Comparison of T_e and T_i space-time evolution

An evolution of T_i is shown on Fig. 5. Now we analyze thin details of T_i and T_e space-time evolution by comparison of Figures 5 and 3. Our goal is to understand similarity of the transport processes of T_i and T_e and to cross-check positions of T_i and T_e measurements. The time resolution of T_i measurements is 17 ms. The total halfwidth of the spatial resolution of T_i measurements is about 7 cm while the same value is 1.7 cm for T_e measured by radiometer.

The sudden rise at the time of event C is seen on T_{i12} (T_{i12} is T_i measured on channel 12). The increase of T_{i12} is saturated at the end of time interval shown on Fig. 5. These features of T_{i12} behavior are exactly similar to the T_{e8-9} evolution. The rise of T_{i13} is seen after $t = 6.635$ s (clearly seen for measurement averaged over 17 ms time interval with center located at $t = 6.653$ s). The increase of T_{e10} is seen after $t = 6.62$ s and the rise of T_{e11} is seen after $t = 6.640$ s. An increase of T_{e12} is not seen in our time interval (up to $t = 6.670$ s). With a position taken with ~ 1 cm outward shift against of space location of T_{e11} we should see T_e evolution (hypotetically measured with T_i space and time resolution) exactly like one can see on $T_{i13}(t)$.

Positions of T_{e1} and T_{e12} were taken equal to 0.37 and 0.66m in reference [10]. Positions of T_i are determined in a magnetic configuration given by an equilibrium calculation with q profiles measured by MSE. Radial locations of T_{i13} and T_{i12} are $r_{i13} = 0.656$ m and $r_{i12} = 0.582$ m. Under above discussed location $r_{i13} = r_{e11} + 1$ cm, position of r_{i12} lies exactly between r_{e8} and r_{e9} ($r_{i12} = r_{i13} - (0.656\text{m} - 0.582\text{m})$), i.e. in right place as discussed above. In reference [10] the value of $r_{e11} + 1$ cm is 1.3 cm less in comparison with r_{i13} value. It means, that under small ~ 1 cm outward shift of r_e reported in [10] against r_i , we should see exactly the same picture of strongly varied in

time and space evolution of T_i and T_e . This small shift is insignificant for analysis reported in present paper and in reference [10]. The space location of r_e against r_i is successfully cross-checked. A complicated but similar behavior of T_i and T_e in space and in time is found. We can prove our result in a longer time interval but this analysis lies outside of a scope of the present paper.

2.3 Experimental picture of heat pulse propagation (HPP)

An evolution of T_e on channels 9-12 is shown in details on Fig. 6. A rising time delay of HPP from channel 9 to 10, from channel 10 to 11, from channel 11 to 12 is clearly seen. Schematic picture of HPP is indicated by an arrows named HPP. A variation of T_e profiles during plasmas evolution after event A is shown in Fig. 7. Profiles of T_e before events A and C are drawn by solid and dashed lines, correspondingly. A propagation of the heat wave front is clearly seen from comparison of T_e profiles, shown in Fig. 7 by dotted lines (16,26,36 ms after C) and by dashed line (66 ms after C).

A similar picture is seen for ion HPP also. A rising time delay of HPP from T_{i12} to T_{i13} and from T_{i13} to T_{i14} is clearly seen in Fig. 5. Schematic picture of HPP is indicated by an arrows named HPP. A variation of T_i profiles during plasmas evolution after event A is shown in Fig. 8. Profiles of T_i before events A and C are drawn by solid and dashed lines, correspondingly. Positions of T_i channels are indicated by squares on solid line. A propagation of the ion heat wave front is clearly seen from comparison of T_i profiles, shown in Fig. 8 by dotted lines (15,31,48 ms after C) and by dashed line (65 ms after C).

3. Analysis of HPP

The first step in HPP analysis is to obtain an experimental value of T_e perturbation $\delta T_{e \text{ EXP}}(r,t)$. An important question is how to subtract slowly

varied in time background temperature $T_{e \text{ BACKGROUND}}(r,t)$ from $T_e(r,t)$ in order to obtain $\delta T_{e \text{ EXP}}(r,t) = T_e(r,t) - T_{e \text{ BACKGROUND}}(r,t)$. An uncertainty of background subtraction is shown in Fig. 6 by dotted lines. The maximum value of T_e perturbation $\delta T_{e \text{ EXP MAX}}(r,t)$ is corresponded to the subtraction of the lower dotted line and vice versa, the minimum value of T_e perturbation $\delta T_{e \text{ EXP MIN}}(r,t)$ is corresponded to the subtraction of the upper dotted line.

A time behavior of $\delta T_{e \text{ EXP}}(r_9, t) \equiv \delta T_{e 9 \text{ EXP}}(t)$ is seen in Fig. 6 as close to linear in 15-20 ms time interval after event C. Detailed variation of $\delta T_{e 9 \text{ EXP}}$ and $\delta T_{e 10 \text{ EXP MAX}}$ with time is shown in Fig. 9 by solid lines.

3.1 Analytical analysis of HPP

In this Section we want to describe briefly analytical method for the study of HPP induced by linear in time perturbation of $T_{i,e}$ and to apply it to the analysis of data described just above. The analytical formulae was published and applied to the analysis of T-10 data [13,15] but the way to obtain it was published in Russian only [14].

Let us analyze the heat transport equation in a straight line geometry :

$$u_t(x,t) = a^2 u_{xx}(x,t) ; x \geq 0 , \quad (3)$$

with initial condition $u(x,0)=0$ and boundary condition $u(0,t) = u_0 t / \tau_0$; $u_t \equiv \partial u / \partial t$, $u_{xx} \equiv \partial^2 u / \partial x^2$. The solution of the Equation (3) is written below :

$$u(x,t) = u(0,t) \Phi(z) ; z = x / (2a \sqrt{t}) , \quad (4)$$

where:

$$\Phi(z) = (2/\sqrt{\pi}) \{ (1+2z^2) I_0(z) (\sqrt{\pi}/2) - z \exp(-z^2) \} , \quad (5)$$

$$I_0(z) = (2/\sqrt{\pi}) \left\{ \int_z^\infty \exp(-y^2) dy \right\} \quad (6)$$

Function

$$\psi = u(x,t) / u(0,t) = \Phi(z) \quad (7)$$

is depended from variable z only. Function $\Phi(z)$ is well approximated by

$$\Phi_1(z) = \exp(-2.5z) \quad (8)$$

in the interval $0 < z < 0.8$.

The ratio of the temperatures in any positions x_2 and x_1

$$\psi_{2,1} \equiv u(x_2,t) / u(x_1,t) = \Phi(z_2) / \Phi(z_1) \quad (9)$$

is not exactly described by dependence from z only. Keeping in mind closeness of $\Phi_1(z)$ and $\Phi(z)$, Equation (9) is rewritten as follows

$$\psi_{2,1} \cong \Phi_1(z_2) / \Phi_1(z_1) = \exp(-2.5(z_2 - z_1)) = \Phi(\Delta_{2,1}) \quad (10)$$

where $\Delta_{2,1} = (x_2 - x_1) / (2a\sqrt{t})$. Therefore, the ratio of the temperatures in any two positions (under $0 < z_{1,2} < 0.8$) is well approximated by the function of one argument z only. Consequently, the algorithm of the thermal diffusivity evaluation from the experimental data measured in two space positions x_2 and x_1 at times t_1 and t_2 is obtained from the Equation (10):

$$(2/3) \chi_e \equiv a^2 = 1.56[(x_2 - x_1)^2 / (t_2 - t_1)] \{ \ln^{-2}(\psi_{2,1}(t_2)) - \ln^{-2}(\psi_{2,1}(t_1)) \}, \quad (11)$$

where x_1 is the position closest to the source of perturbation (higher amplitude of the temperature).

The formulae (11) is written for the general case covered by Equation (3) with linear in time boundary condition. We can use it for HPP study with replacement of $u(x,t)$ to $\delta T_e(r,t)$. Keeping in mind possible difference of χ_e^{PB} , χ_e and χ_e^{HP} described in introduction, it is also necessary to replace χ_e to χ_e^{HP} . For the study of HPP from linear in time $\delta T_e(r_1, t)$ it is necessary to correct slightly $\psi_{2,1}$ function in Equations (9,11) for cylindrical geometry as was shown by numerical calculations in [14]:

$$\psi_{2,1} \equiv [\delta T_e(r_2, t) / \delta T_e(r_1, t)] (r_1 / r_2)^{0.5} \quad (12)$$

and to replace x_2, x_1 to r_2, r_1 . In order to take approximately into account the variation of n_e , expression (12) should be multiplied by $(n_e(r_1) / n_e(r_2))^{0.5}$

value. Corrections described above are insignificant usually. The formulae (11) was checked with transport code calculations for the various conditions [14] and was used for the analysis of ECRH induced HPP on T-10 [15]. The results obtained were in good agreement with full transport code calculations [15]. The best time interval for the analysis of the experimental data was found as the interval $0.15 \leq \psi_{2,1} \leq 0.4$ [14].

It is not always easy to measure the ratio of temperatures in two points exactly correctly in time. It is clearly seen from Fig. 6 that it is easier (means less error bars) to define start time of the linear temperature variation at the position r_1 ($r(\text{ch.9})$) and to identify time when $\psi_{2,1} = 0.4$ or 0.3 . Equation (11) is rewritten for one time point. Using small corrections from full Equations (3-5), the new expression for χ_e^{HP} is obtained :

$$\chi_e^{\text{HP}} = C(\psi_{2,1}) [(r_2 - r_1)^2 / \Delta t] / \ln^2(\psi_{2,1}(\Delta t)) \quad (13)$$

where Δt is the time interval passed from the start of the linear variation at the position r_1 and $C(\psi_{2,1}) = 2.3, 2.41, 2.59$ for $\psi_{2,1} = 0.4, 0.3, 0.2$, consequently. The optimum $0.3 \leq \psi_{2,1} \leq 0.4$ interval is determined for Equation (13).

The values of $\chi_e^{\text{HP}} = 0.11, 0.08, 0.1 \text{ m}^2/\text{s}$ are obtained with Equation (13) from ratio of $\delta T_{e10 \text{ EXP MAX}}(t)$ and $\delta T_{e9 \text{ EXP}}(t)$ taken from Fig. 6 for $\Delta t = 10, 15, 20 \text{ ms}$, respectively. The values of $\chi_e^{\text{HP}} = 0.055$ and $0.065 \text{ m}^2/\text{s}$ are determined with Equation (13) from ratio of $\delta T_{e10 \text{ EXP MIN}}(t)$ and $\delta T_{e9 \text{ EXP}}(t)$ for $\Delta t = 20$ and 26 ms , correspondingly.

3.2. Numerical analysis of HPP

Regarding perturbations of heat sources and n_e , HPP is analyzed with simplified transport equation for δT_e , as usually :

$$1.5n_e \partial \delta T_e / \partial t = - \text{div} (n_e \chi_e^{\text{HP}} \nabla \delta T_e), r_1 \leq r \leq r_{\text{sep}}, \quad (14)$$

with zero initial condition $\delta T_e(r, 0) = 0$. Left boundary condition $\delta T_e(r_1, t)$ is taken from the experimental measurements at $r = r_1$: $\delta T_{e \text{ CALC}}(r_1, t) = \delta T_{e \text{ EXP}}(r_1, t)$. Right boundary condition is chosen as zero on separatrix radius $\delta T_{e \text{ CALC}}(r_{\text{sep}}, t) = 0$. Profile $n_e(r)$ is taken from experiment. The calculated perturbation $\delta T_{e \text{ CALC}}(r_{2i}, t)$, where r_{2i} ($i=1, N$) are radii of comparison of the $\delta T_{e \text{ CALC}}(r_{2i}, t)$ and $\delta T_{e \text{ EXP}}(r_{2i}, t)$, is depended from χ_e^{HP} : $\delta T_{e \text{ CALC}}(r_{2i}, t) = \delta T_{e \text{ CALC}}(\chi_e^{\text{HP}}, r_{2i}, t)$. The optimum value χ_e^{HP} is determined automatically from the best fit to the calculated and experimental data by minimizing the difference

$$M = \sum_{i=1}^N \int_0^{\Delta t} [\delta T_{e \text{ CALC}}(\chi_e^{\text{HP}}, r_{2i}, t) - \delta T_{e \text{ EXP}}(r_{2i}, t)]^2 dt$$

Equation (14) is solved using an implicit conservative difference scheme described in [34]. The difference problem is solved with a three point Gauss eliminating method described anywhere including [34].

Examples of the solution of Equation (14) for three different values of χ_e^{HP} are shown in Fig (9). In this case $r_1 = r(\text{ch.9}) \equiv r_{e9}$, $r_2 = r(\text{ch.10}) \equiv r_{e10}$, $\delta T_{e \text{ EXP}}(r_{10}, t) = \delta T_{e \text{ EXP MAX}}(r_{10}, t)$ are taken. The best fit is obtained with $\chi_e^{\text{HP}} = 0.1 \text{ m}^2/\text{s}$ (for $\Delta t = 35 \text{ ms}$). Further we will call such an optimum value an “obtained value”. The values of $\chi_e^{\text{HP}} = 0.12$ and $0.08 \text{ m}^2/\text{s}$ are obtained for $\Delta t = 45 \text{ ms}$ and $\Delta t = 25 \text{ ms}$, respectively.

For the same calculations with $\delta T_{e \text{ EXP}}(r_{10}, t) = \delta T_{e \text{ EXP MIN}}(r_{10}, t)$ corresponded values of χ_e^{HP} are near $0.04 \text{ m}^2/\text{s}$ for $\Delta t = 35 \text{ ms}$ and 25 ms . All values reported above are in reasonable agreement with χ_e^{HP} values obtained analytically in Section 3.1.

An important experimentally measured characteristic of HPP is described by the index of “quality” of a heat wave first time introduced in [21,22]. The index is the “relative sharpness” of the heat wave and is defined:

$$\langle S \rangle = \langle |(\delta \nabla T_e / \delta T_e) / (\nabla T_e / T_e)| \rangle \quad (15)$$

where brackets $\langle \rangle$ denote time averaged quantity. This is the experimental characterization of the sensitivity of conduction term ($\chi_e^{\text{HP}} \delta \nabla T_e$) to “convective-like” terms (source perturbation, gradual dependencies of χ_e from t and T_e , etc.). The value of S is decreased in time due to a diffusive spreading of the perturbation. This is one of the reason why the HPP study is bounded in time. Not- averaged in time values of the $S(\text{ch.9} - \text{ch.10}, t)$ equal to 10.3, 6.9, 5.1, 2.7 are obtained for $\Delta t = 16, 26, 36, 46$ ms after event C, consequently. The same values for $S(\text{ch.10} - \text{ch.11}) = 11.7, 10.4, 7.9, 7.3$ are found. These values should be treated as very high because values of S for sawteeth induced HPP study on JET were equal to 2 or 3 usually [29]. It means that we have high quality HPP. The space region of the high S values is moved outside with time. It is the reason why we describe first not HPP study from ch. 9 to ch. 10,11,12 simultaneously in $\Delta t = 60$ ms or 70 ms time interval, but HPP study from ch. 10 to 11, from ch. 11 to 12 in a different Δt values.

Now we study HPP from channel 10 to channel 11. Values of $\delta T_{e \text{ EXP MAX}}(r_{e 10}, t)$ and $\delta T_{e \text{ EXP MAX}}(r_{e 11}, t)$ are shown by solid lines in Fig. 10. Timetraces of $\delta T_{e \text{ CALC}}(r_{e 11}, t)$ calculated with $\delta T_{e \text{ EXP}}(r_1, t) = \delta T_{e \text{ EXP MAX}}(r_{e 10}, t)$ and $\delta T_{e \text{ EXP}}(r_2, t) = \delta T_{e \text{ EXP MAX}}(r_{e 11}, t)$ for three different value of χ_e^{HP} are shown by dotted lines. Values of $\chi_e^{\text{HP}} = 0.105$ and $0.1 \text{ m}^2/\text{s}$ are obtained for $\Delta t = 45$ ms and $\Delta t = 35$ ms, correspondingly. Values of $\chi_e^{\text{HP}} = 0.053$ and $0.058 \text{ m}^2/\text{s}$ are derived for the same time intervals with $\delta T_{e \text{ EXP}}(r_1, t) = \delta T_{e \text{ EXP MIN}}(r_{e 10}, t)$ and $\delta T_{e \text{ EXP}}(r_2, t) = \delta T_{e \text{ EXP MIN}}(r_{e 11}, t)$ and lower quantities $\chi_e^{\text{HP}} = 0.036$ and $0.037 \text{ m}^2/\text{s}$ obtained with $\delta T_{e \text{ EXP}}(r_1, t) = \delta T_{e \text{ EXP MAX}}(r_{e 10}, t)$ and $\delta T_{e \text{ EXP}}(r_2, t) = \delta T_{e \text{ EXP MIN}}(r_{e 11}, t)$. Naturally, higher values $\chi_e^{\text{HP}} = 0.21$ and $0.23 \text{ m}^2/\text{s}$ are derived with $\delta T_{e \text{ EXP}}(r_1, t) = \delta T_{e \text{ EXP MIN}}(r_{e 10}, t)$ and $\delta T_{e \text{ EXP}}(r_2, t) = \delta T_{e \text{ EXP MAX}}(r_{e 11}, t)$.

For HPP from ch. 11 to ch.12, values of χ_e^{HP} equal to 0.055 and 0.06 m^2/s are obtained for $\Delta t = 55 \text{ ms}$ and $\Delta t = 45 \text{ ms}$ time intervals with $\delta T_{e \text{ EXP}}(r_1, t) = \delta T_{e \text{ EXP MAX}}(r_{e 11}, t)$ and $\delta T_{e \text{ EXP}}(r_2, t) = \delta T_{e \text{ EXP MAX}}(r_{e 12}, t)$.

A sensitivity of the χ_e^{HP} values obtained above to a method of the $T_{e \text{ BACKGROUND}}(r, t)$ subtraction obviously follows from the analysis reported above. The behavior of $\delta T_e(r_{e 10, 11, 12}, t)$ shown in Fig. 6 is seen as quiet gradual evolution after event C and is well described by the diffusive picture of HPP from $\delta T_e(r_{e 9}, t)$. We have no single evidence to suppose a strongly varied behavior of $T_{e \text{ BACKGROUND}}(r_{e 10, 11, 12}, t)$. Obviously, upper values of χ_e^{HP} obtained above with $\delta T_{e \text{ EXP}}(r_1, t) = \delta T_{e \text{ EXP MIN}}(r_{e n}, t)$ and $\delta T_{e \text{ EXP}}(r_2, t) = \delta T_{e \text{ EXP MAX}}(r_{e n+1}, t)$ should be treated as overestimated upper limit of χ_e^{HP} . Similarly, lower values of χ_e^{HP} obtained above with $\delta T_{e \text{ EXP}}(r_1, t) = \delta T_{e \text{ EXP MAX}}(r_{e n}, t)$ and $\delta T_{e \text{ EXP}}(r_2, t) = \delta T_{e \text{ EXP MIN}}(r_{e n+1}, t)$ should be considered as underestimated lower limit of χ_e^{HP} . By our opinion, χ_e^{HP} obtained above with $\delta T_{e \text{ EXP}}(r_1, t) = \delta T_{e \text{ EXP MAX}}(r_{e n}, t)$ and $\delta T_{e \text{ EXP}}(r_2, t) = \delta T_{e \text{ EXP MAX}}(r_{e n+1}, t)$ should be treated as "real" values of χ_e^{HP} .

A sensitivity of calculated data from χ_e^{HP} values increases with a rise of a width of HPP study region. An example of HPP from $r_{e 9}$ to $r_{e 11}$ is shown in Fig. 11. The timetraces of the $\delta T_{e \text{ EXP MAX}}$ for $r_{e 9}$, $r_{e 10}$, $r_{e 11}$ are shown by solid lines. Left boundary condition is located on $r_{e 9}$ position : $\delta T_{e \text{ EXP}}(r_1, t) = \delta T_{e \text{ EXP MAX}}(r_{e 9}, t)$. An evolution of $\delta T_{e \text{ CALC}}$ at $r_{e 10}$ and $r_{e 11}$ radii calculated with $\chi_e^{\text{HP}} = 0.1 \text{ m}^2/\text{s}$ are drawn by dotted lines. Values of $\delta T_{e \text{ CALC}}(r_{e 11}, t)$ with $\chi_e^{\text{HP}} = 0.2$ and $0.05 \text{ m}^2/\text{s}$ are shown in Fig. 11 by dashed lines. A larger deviation of dashed lines from $\delta T_{e \text{ EXP}}(r_{e 11}, t)$ in Fig. 11 is clearly seen from comparison with the same deviation shown in Fig.10 by dashed lines also.

Now it is the time to discuss the sensitivity of χ_e^{HP} values obtained above inside $r_9 \leq r \leq r_{12}$ space region from an unknown profile of $\chi_e^{\text{HP}}(r)$ in $r_{12} \leq r \leq r_{\text{sep}}$ space zone and from really uncertain type of a boundary condition for δT_e on separatrix radius r_{sep} . An exact type of boundary condition on separatrix is absolutely not important because HPP does not “feel” it during ~60 ms time interval studied above. The heat wave is almost not seen at channel 12 and r_{sep} is located far enough from r_{e12} . Naturally, the region most sensitive to an uncertainty of $\chi_e^{\text{HP}}(r)$ in $r_{12} \leq r \leq r_{\text{sep}}$ zone is located between r_{11} and r_{12} . Calculations with various profiles of $\chi_e^{\text{HP}}(r)$ in $r_{12} \leq r \leq r_{\text{sep}}$ are carried out. An influence of unknown $\chi_e^{\text{HP}}(r \geq r_{12})$ is seen in $r_{11} \leq r \leq r_{12}$ space region, but almost not seen in $r_9 \leq r \leq r_{11}$ zone. For example, HPP is studied with radial profile of χ_e^{HP} given as follows

$$\chi_e^{\text{HP}}(r) = \chi_{e0}^{\text{HP}} \text{ for } r \leq r_{12}, \quad (16)$$

$$\chi_e^{\text{HP}}(r) = \chi_{e0}^{\text{HP}} + \{(r - r_{12}) / (0.05\text{m})\} \text{ m}^2/\text{s} \text{ for } r_{12} \leq r \leq r_{\text{sep}}, \quad (17)$$

i.e. with strong rise (1m²/s per 5 cm distance) of $\chi_e^{\text{HP}}(r)$ along r for $r \geq r_{12}$. A value of χ_{e0}^{HP} is varied in Equations (16 - 17) in order to obtain the best fit.

For HPP from ch. 11 to ch.12, values of $\chi_{e0}^{\text{HP}} = 0.1$ and $0.11 \text{ m}^2/\text{s}$ are obtained for $\Delta t = 55 \text{ ms}$ and $\Delta t = 45 \text{ ms}$ time intervals with $\delta T_{e \text{ EXP}}(r_1, t) = \delta T_{e \text{ EXP MAX}}(r_{e11}, t)$ and $\delta T_{e \text{ EXP}}(r_2, t) = \delta T_{e \text{ EXP MAX}}(r_{e12}, t)$, i.e. nearly 2 times higher in comparison with that of reported above without radial dependence of $\chi_e^{\text{HP}}(r)$. It is found that HPP in zone $r_9 \leq r \leq r_{11}$ is almost insensitive to an uncertainty of $\chi_e^{\text{HP}}(r)$ in $r_{12} \leq r \leq r_{\text{sep}}$ zone.

In general, an errorbar level is estimated as $\chi_e^{\text{HP}} = 0.1 (0.05 \div 0.17) \text{ m}^2/\text{s}$ in the region of HPP study.

Ion HPP should be analyzed keeping in mind low spatial resolution (~7cm) and low time resolution (17ms) of $T_i(r, t)$ measurements. As already

discussed in the end of Section 2, a rising time delay of ion HPP from T_{i12} to T_{i13} and from T_{i13} to T_{i14} is seen in Fig. 5. The distance between channels is equal to 7.5 cm. Under the more careful view, the immediate response to the event C is clearly observed for T_{i13} in Fig. 5. For HPP from r_{i12} to r_{i13} in $\Delta t = 30$ ms time interval, values $\chi_i^{\text{HP}} \cong 0.4 \text{ m}^2/\text{s}$ are found. The “real distance” between r_{i13} and r_{i12} defined from HPP analysis point of view should not be taken equal to $r_{i13} - r_{i12}$ by an obvious reason connected with 7cm spatial resolution. Immediate rise of δT_i is seen around r_{i12} location as shown in Section 2.2. A value of δT_{i13} should “feel” HPP by inner boundary of its space resolution region. It means that the “real distance” is approximately equal to the width of the zone between outer edge of the zone of immediate δT_i rise around r_{i12} and inner boundary of channel 13 space resolution region, i.e. equal to a few but not to 7.5 cm. Roughly speaking, χ_i^{HP} should be reduced by 4 times under 2 times reduction of “real distance” between r_{i12} and r_{i13} . High values of χ_i^{HP} found for HPP between r_{i12} and r_{i13} are explained.

An influence of space resolution on HPP analysis from r_{i13} to r_{i14} should be less seen in comparison with that of from channel 12 to 13. HPP is observed as gradual process of heat wave propagation from left space resolution boundary of channel 13 to the same boundary of channel 14. Values of $\chi_i^{\text{HP}} = 0.14 \text{ m}^2/\text{s}$ are obtained for $\Delta t = 67$ ms and $\Delta t = 50$ ms time intervals. The value of $\langle S \rangle$ is high and is equal to 5 for $\Delta t = 67$ ms. In general, an errorbar level is estimated as $\chi_i^{\text{HP}} = 0.14 (0.08 \div 0.25) \text{ m}^2/\text{s}$.

4. Consequences for heat flux structure

Values of χ_e^{HP} reported in the Section 3 are obtained from analytical and numerical solutions of simplified Equation (14). An Equation (1) is a full equation for the transport description of any $\delta T_e(r, t)$ with non varying heat

sources or sinks. Reminding that in simplified Equation (14) value of $n_e \chi_e^{\text{HP}}$ $\delta \nabla T_e$ should be equal to a full perturbation of the electron heat flux $\delta \Gamma_e$, Equations (1) and (14) are rewritten as

$$1.5n_e \delta \partial T_e / \partial t = - \text{div} \{ n_e [\delta \chi_e \nabla T_e + (\chi_e + \delta \chi_e) \delta \nabla T_e] \} = - \text{div} \{ n_e \chi_e^{\text{HP}} \delta \nabla T_e \} \quad (18)$$

Therefore, expression for χ_e^{HP} is obtained from Equation (18) as follows

$$\chi_e^{\text{HP}} \delta \nabla T_e = \delta \chi_e \nabla T_e + (\chi_e + \delta \chi_e) \delta \nabla T_e \equiv -\delta \Gamma_e \quad , \quad (19)$$

$$\chi_e^{\text{HP}} = \delta \chi_e \nabla T_e / \delta \nabla T_e + \chi_e + \delta \chi_e \quad . \quad (20)$$

The diffusive picture of HPP, however, is not affected by χ_e dependence on ∇T_e , i.e. $\delta \chi_e = (\partial \chi_e / \partial \nabla T_e) \delta \nabla T_e$, since Equation (20) could be rewritten (under $\delta \nabla T_e / \nabla T_e \ll 1$) as [11] :

$$\chi_e^{\text{HP}} = \chi_e + (\partial \chi_e / \partial \nabla T_e) \nabla T_e \quad . \quad (21)$$

In principle, depending from sign of $\partial \chi_e / \partial \nabla T_e$, one can obtain from Equation (21) or $\chi_e^{\text{HP}} \gg \chi_e$ (“enhanced HPP”), or $\chi_e^{\text{HP}} \ll \chi_e$ (“reduced HPP”). Such an explanation was suggested in [26] for an interpretation of reduced HPP seen in one of T-10 regimes. Our new interpretation of these T-10 results is given below in Section 5. Strictly speaking, we can not fully reject the same explanation and for JT-60U results reported in Section 3. But we do not see any physical reason for it.

Real χ_e in plasmas is equal to χ_e measured with power balance χ_e^{PB} in any case besides existence of “heat pinch”. For “simple heat pinch” case electron heat flux Γ_e is described by expression

$$\Gamma_e = -n_e (\chi_e \nabla T_e + V_{Te} T_e) \quad (22)$$

where V_{Te} is inward convective velocity or heat pinch velocity. The value of $\chi_e^{PB} \equiv -\Gamma_e / \nabla T_e$ in this case is not equal, but smaller than that of χ_e . If χ_e and V_{Te} are not varied during HPP, $\delta\Gamma_e$ is expressed from Equation (22) as

$$\delta\Gamma_e = -n_e (\chi_e \delta\nabla T_e + V_{Te} \delta T_e) . \quad (23)$$

A value of χ_e^{HP} is obtained from Equation (23) as

$$\chi_e^{HP} \equiv -\delta\Gamma_e / (n_e \delta\nabla T_e) = \chi_e + V_{Te} \delta T_e / \delta\nabla T_e . \quad (24)$$

A main idea of heat pinch is that two terms in RHS of the Equation (22) are almost compensated in steady state case, i.e.

$$\chi_e \nabla T_e \equiv -V_{Te} T_e . \quad (25)$$

After substituting Equation (25) into Equation (24), it is rewritten as

$$\chi_e^{HP} = \chi_e + V_{Te} \delta T_e / \delta\nabla T_e \equiv \chi_e [1 - (\nabla T_e / T_e) (\delta\nabla T_e / \delta T_e)] \quad (26)$$

For the first time Equation (26) was obtained in [11] and its applicability for HPP study was checked with transport code calculations. Keeping in mind Equation (15) for an index of quality of HPP S, Equation (24) now is written as

$$\chi_e^{HP} = \chi_e [1 - 1 / S] . \quad (27)$$

By introducing a factor of disbalanement of heat fluxes in the Equation (22) β , Equations (25) and (27) are presented in more accurate form as

$$V_{Te} T_e = -(1-\beta) \chi_e \nabla T_e \quad (28)$$

$$\chi_e^{HP} = \chi_e [1 - (1-\beta) / S] . \quad (29)$$

For $\beta = 1$ heat pinch is absent and for $\beta = 0.1$ convective heat flux is equal to 90% of conductive heat flux (or $\chi_e^{PB} = 0.1 \chi_e$).

Keeping in mind Equations (22-27), now we analyze V_{Te} values for results described in Section 3. The basic value of $\chi_e^{HP} = 0.1 \text{ m}^2/\text{s}$ is taken now. A values of $1/\langle S \rangle$ (see Equation (15)) are low enough to be small (0.1-0.2) varied in time correction in the Equation (27). For example, in case of HPP from $\delta T_{e \text{ EXP}}(r_9, t)$ to $\delta T_{e \text{ EXP MAX}}(r_{10}, t)$ in time interval $\Delta t = 35 \text{ ms}$, the value of $1/\langle S \rangle$ is equal to 0.15. By substituting expression for χ_e taken from Equation (29) for χ_e in Equation (28) an expression for V_{Te} is obtained

$$V_{Te} = -\chi_e^{HP} [(1-\beta)/(1-(1-\beta)/S)] (\nabla T_e / T_e) \quad (30)$$

A term in square brackets is close to 1 or less than 1 for $0.1 < \beta < 1$. An upper limit of this term for $0 < \beta < 1$ is equal to $1/(1-1/S) \cong 1 + 1/S$ for high values of S . A Set of Equations (28-30) is valid for HPP with large values of $\delta \nabla T_e$ also. The main uncertainty in the Equation (30) is connected with a value of ∇T_e which is probably overestimated in the region $r_{e8} < r < r_{e12}$ in present paper (see discussion about it in Section 2). That is why the value of V_{Te} is probably overestimated with $(\nabla T_e / T_e)$ taken from Fig. 7 also. Values of $V_{Te} \cong -0.4 \text{ m/s}$ are obtained from Equation (30) for all region of electron HPP study.

A value of $V_{Te} = -0.35 \text{ m/s}$ is obtained from Equation (30) for ion HPP from the ion channel 13 to the ion channel 14.

5. Discussion

We want to try to interpret now surprisingly low value of $\chi_e^{HP} = 0.14 \text{ m}^2/\text{s}$ which was obtained in one of the regimes on T-10 [26] (already briefly described in Section 1). The reason to discuss it here is that for many years this L-mode result was a "single point" without any reasonable explanation. It is the

only one known in the world result similar to HPP study described in the present paper.

The outward HPP was created by on-axis ECRH (0.4 MW of the absorbed EC power) imposed on a broad steady state background T_e profile sustained by off-axis ECRH (0.9 MW of the absorbed EC power) switched-on 100 ms before. Sawteeth oscillations in this low- q regime ($I_p = 0.4$ MA, $q=2.2$ on liner, $B_t = 3$ T) were almost instantly suppressed by off-axis ECRH switching-on. The $\chi_e^{\text{HP}} = 0.14$ (0.08 - 0.2) m^2/s value was obtained in 2 cm spatial zone (at 0.45 of r/a) located near former sawteeth “mixing radius”. It is known, that “sawteeth double reconnection model” [35] is usually capable to describe sawteeth oscillations on T-10, even in low- q regimes [36]. There are two $q=1$ surfaces in this model because q profile is not monotonical outside sawteeth inversion radius. The first $q=1$ surface lies on the inversion radius position and the second one lies on the “mixing radius” position i.e. exactly in the spatial region of HPP study.

The current profile $j(r)$ was almost frozen and just slightly redistributed and broaden during 100 ms sawteeth suppression phase because of high temperature ($T_e(0) = 4$ keV) and broad T_e profile created [38] (broader in comparison with the ohmic one). We can expect an existence of the low shear region near $q=1$ surface in the experiment described above. Recent results of T-10 [37] shows existence of ITBs near rational q surfaces under the low shear created by ECCD around these surfaces.

Now we can interpret 10 years old T-10 result with “superlow” value of $\chi_e^{\text{HP}} = 0.14$ m^2/s [26] as the first evidence of the ITB existence. The “superlow” value of χ_e^{HP} was measured in 2 cm zone (0.06 of minor radius) inside ITB located in the low-shear region around $q=1$ surface. A total width of the ITB layer was not measured.

We want to estimate now the value of the “heat pinch” velocity for this T-10 case. An absence of “significant heat pinch” was claimed in [26,38], but

an absolute value was not reported. By taking T_e profile from [38], we obtain -0.5 m/s value of the convective heat velocity with method described in Section 4. Values of the local T_e and n_e in the T-10 case are 1.5 and around 3 times higher correspondingly, in comparison with those values in the region of JT-60U HPP study described above.

A region of improved confinement inside or, probably, including $q=1$ surface was seen after pellet injection in JT-60 [39].

Sometimes one can find in a literature a statement about existence of a large “heat pinch” with tens m/s order of magnitude of an inward velocity. A convective heat velocity order of 60 m/s was claimed recently for ECRH induced HPP throughout ITB’s formed near rational q surfaces in RTP [40].

By our knowledge of T-10, JET, JT-60U data, there are no one direct evidence of the significant heat pinch existence in any confinement regime. Moreover, as we describe for RS regime of JT-60U in present paper and as was obtained before on T-10 and JET in another regimes [22, 24-26] described in Section 1, there are direct evidences of the absence of a heat pinch in all various regimes with improved electron confinement studied so far. Small values of inward convective heat velocity of order of 0.5 m/s (for T-10 it is compatible with neoclassical inward convective electron density velocity called sometimes “ particle pinch velocity”, see reference [36]), i.e. two orders of amplitude less than that claimed in RTP [40], could be discussed only.

Nevertheless, an existence or an absence of a large “heat pinch” in usual L mode is still not a fully answered question.

Values of χ_e^{HP} obtained above are not sensitive to values of ∇T_e because χ_e^{HP} values are sensitive to the ratio of δT_e on neighboring radiometer channels. This ratio is almost not sensitive to variation of ∇T_e values (8% variation of the ratio and corresponded 14% variation of χ_e^{HP} for two times variation of ∇T_e). And, vice versa, values of V_{T_e} and of event-created $\delta\chi_e$ are inversely proportional to ∇T_e .

Results described in present paper are the first step only. We hope to clarify ITB transport properties in various regimes and in various shear zones with an analysis of inward and outward HPP that should be done in the nearest future.

6. Summary

A new source of heat pulse propagation is found in JT-60U RS plasmas. Abrupt in time and wide in space variations of heat diffusivity ("events") were recently described in details in JT-60U RS plasmas [10]. An evolution of the ITB during 100 ms time interval after strong ITB formation is described. The first event is occurred 35 ms after strong ITB formation. It is ITB partial degradation. The second event (ITB improvement) is occurred 10 ms later. The spatial zone covered by the second event is shifted outside in comparison with the first one and is fully located in positive shear zone. The sum result of two events is an outward shift of the improved confinement zone.

The behavior of $T_{e,i}(r,t)$ is strongly varied in time and very sharply in space during 100 ms time interval discussed in this paper. The space positions of the channels for T_e and T_i measurements against each other are confirmed independently from equilibrium calculations by comparison of an evolution of $T_e(r,t)$ and $T_i(r,t)$.

For the second event the region of strong (~ 20 keV/s) T_e rise is well localized (~ 4 cm) in space initially. Later in time, a slow diffusive broadening of the rising T_e perturbation, or an outward motion of a heat wave front, is seen. In other words, it is a clear picture of outward heat pulse propagation (HPP) created by event . It is HPP throughout ITB region with confinement abruptly improved by this event.

A slightly modified analytical method for the study of HPP induced by linear in time perturbation of the temperature is described. HPP is analyzed analytically and numerically. Similar results are obtained with both methods.

The “quality” or the “sharpness” of the heat wave is high due to well localized in space region of T_e rise. Values of the electron heat diffusivity as low as $\sim 0.1 \text{ m}^2/\text{s}$ are found in the region with $\sim 8 \text{ cm}$ width. Ion HPP is analyzed in slightly shifted outward zone in comparison with electron HPP space region. A similar low values of the ion heat diffusivity ($\sim 0.14 \text{ m}^2/\text{s}$) are obtained. It is the first study of HPP in RS plasmas of any tokamak and the first study of ITB properties in positive shear space zone of JT-60U RS plasmas.

An important consequence of HPP analysis for an anomalous heat flux structure is an absence of electron and ion “heat pinch” in the ITB region. The low -0.4 m/s value of the permitted electron convective inward heat velocity is obtained. The same -0.35 m/s value is found for the ion inward convective heat velocity

Acknowledgments

The authors express their gratitude to Drs. M. Azumi, A. Funahashi, M. Kikuchi, H. Ninomiya, T. Ozeki and R. Yoshino for their continuous encouragements. They also thank Drs. T. Fukuda, S. Ide, N. Isei, T. Hatae, T. Oikawa and many other members of JT-60U team for their fruitful discussion and fine collaboration. One of the authors (S. V. N.) want to express his gratitude to Prof. Y. N. Dnestrovskii for many years of collaboration and encouragement of HPP analysis started by S. V. N. 15 years ago on T-10. He also wants to thank Dr. M. I. Mironov for his help in UNIX system. This work was carried out during S. V. N.'s stay at JAERI under JAERI Research Fellowship.

References

- [1] T. Fujita, Y. Kamada Y, S. Ishida et al, 1998, 17th IAEA Fusion Energy Conf. (Yokohama, 1998) IAEA-CN-69/EX1/2; to be published in Nucl. Fusion
- [2] Y. Kamada, A. Isayama, T. Oikawa et al., 1998, 17th IAEA Fusion Energy Conf. (Yokohama, 1998) IAEA-CN-69/CD2/EX1/2; to be published in Nucl. Fusion
- [3] Y. Shimomura, R. Aymar, V. Chyanov et al, 1998, 17th IAEA Fusion Energy Conf.(Yokohama, 1998) IAEA-CN-69/OV4/1
- [4] Y. Koide, M. Mori, T. Fujita et al, 1998, Plasma Phys. Control. Fusion **40**, 641
- [5] H. Shirai, M. Kikuchi, T. Takizuka et al, 1998, 17th IAEA Fusion Energy Conf. (Yokohama, 1998) IAEA-CN-69/EX5/4; to be published in Nucl. Fusion
- [6] T. Fujita, S. Ide, H. Kimura et al, 1997, Fusion Energy 1996, Proc. 16th Int. Conf. (Montreal, 1996) vol 1 (Vienna: IAEA) p 227
- [7] S. V. Neudatchin, T. Takizuka, H. Shirai, T. Fujita, S. Takeji, N. Isei and Y. Kamada, "Analysis of Space-Time Structure of Internal Transport Barrier in JT-60U" 1997, JAERI-Research 97-052
- [8] S. V. Neudatchin, H. Shirai, T. Takizuka, T. Fujita, S. Takeji, N. Isei and Y. Kamada, Proc. 24th EPS Conf. on Controlled Fusion and Plasma Physics (Berchtesgaden, 1997), vol. 21A (Geneva:EPS), part II, p. 497
- [9] S. V. Neudatchin, T. Takizuka, H. Shirai, T. Fujita, N. Isei, Y. Koide, T. Oikawa, T. Hatae, and Y. Kamada - in: Meeting Abstracts of the Phys. Soc. of Japan (1999), vol. 54, issue 1, part 4, p. 820
- [10] S. V. Neudatchin, T. Takizuka, H. Shirai, T. Fujita, N. Isei, A. Isayama, Y. Koide and Y. Kamada, Plasma Phys. Control. Fusion **41** (1999) L39
- [11] S.V. Neudatchin, "Influence of Electron Temperature Perturbations on Electron Heat Diffusivity in a Tokamak", in: "Voprosy Atomnoi Nauki i Tekhniki" (Questions of Atomic Science and Engineering, Thermonuclear Fusion Series) (in Russian), (1986), issue 3, p. 39
- [12] J. D. Callen, J. P. Christiansen, J. G. Cordey, et al, 1987, Nucl. Fusion **27** 1857
- [13] T-10 Group, Proc. 12th EPS Conf. on Contr. Fusion and Plasma Heating (Budapest, 1985), vol. 9F (Geneva:EPS), part II, p. 38
- [14] Y.N. Dnestrovskij and S.V. Neudatchin : "Determination of Electron Heat Diffusivity Coefficient by Characteristics of Heat Wave Induced by ECR Heating", Kurchatov Institute of Atomic Energy Report IAE -4301/6 (1986) (in Russian)
- [15]* A.A. Bagdasarov, N.L. Vasin, Y.V. Esipchik, S.V. Neudatchin, K.A. Razumova, P.V. Savrukhin, K. N. Tarasyan, Soviet J. Plasma Phys., **13**(8),517 (1987)
- [16] S. V. Neudatchin, Proc, 15th Eur. Conf. on Contr. Fus and Plasma Heating (Dubrovnik,1988), vol. 12B (Geneva:EPS), part III, p. 1147
- [17] J. D. Callen, G. L. Jans, Phys. Rev. Lett., **38** (1977) 491
- [18] E. D. Fredrikson, J. D. Callen, K. McGuire, et al., Nucl. Fusion, **26** (1986) 849.
- [19] K. Riedel, A. Eberhagen, O. Gruber, et al., Nucl. Fusion, **28** (1988) 1509.
- [20] A.A. Bagdasarov and S.V. Neudatchin, Proc. 18th European Conf. on Contr. Fusion and Plasma Physics (Berlin 1991) vol. 15C (Geneva:EPS) part II, p. 101
- [21] Neudatchin S. V. , Cordey J. G. and Muir D. G., Proc. 20th EPS Conf. on Controlled Fusion and Plasma Physics (Lisboa, 1993) part I (Geneva:EPS), p. 83

- [22] S.V. Neudatchin and D. G. Muir, "The Study of Electron Heat Transport in JET by Analysing the Decay of Temperature Perturbations induced by Sawteeth", JET-P (93) 27 (1993)
- [23] E. D. Fredrickson, K. McGuire, A. Gavallo, et al., Phys. Rev. Lett., **65**, (1990), 2869
- [24] V. V. Alikaev, A. A. Bagdasarov, E. L. Beresovskij, et al, in : Plasma Phys. and Control. Nuclear Fusion Research (Proc. 11th Int. Conf., Kyoto, 1986), vol. 1, IAEA, Vienna (1987) p. 111.
- [25] B. Balet, D. Boucher, J.G. Cordey, D. G. Muir, S.V. Neudatchin, G. Shmidt, in: Proc. 19th European Conf. on Control. Fusion and Plasma Phys. (Innsbruck1992) vol. 16C (Geneva:EPS) part I, p. 59
- [26]* A. A. Bagdasarov, N. L. Vasin, S. V. Neudatchin, P. V. Savrukhnin, in Plasma Phys. and Control. Nuclear Fusion Research (Proc. 15th Int. Conf., Washington, 1990), vol. 1, IAEA, Vienna (1991) p. 253
- [27] Y.N. Dnestrovskii, E. L. Beresovskii, S. E Lysenko, et al, Nucl Fusion **30** (1990) 1475.
- [28] Y.N. Dnestrovskii, S. E. Lysenko, K. N. Tarasyan, A. R. Polevoi, H. Shirai, T. Takizuka, M. Kikuchi, 17th IAEA Fusion Energy Conf. (Yokohama, 1998) IAEA-CN69-THP2/17, to be published in Nuclear Fusion
- [29] S.V. Neudatchin , J.G. Cordey and D. Muir "The time behaviour of the electron conductivity during L-H and H-L transitions in JET", JET-P (93) 27 (1993)
- [30] S. V. Neudatchin S, T. Takizuka, H. Shirai, N. Isei, Y. Kamada, Y.Koide, M. Sato and M. Azumi, 1996, Jpn. J. Appl. Phys. **35**, 3595
- [31] J. G. Cordey, D. G. Muir, S. V. Neudatchin, et al, Plasma Phys. Control. Fusion, **36** (1994) Suppl. A267
- [32] Y. Koide, T. Fujita, T. Takizuka et al, 1998, 17th IAEA Fusion Energy Conf. (Yokohama, 1998) IAEA-F1-CN-69/EX5/2
- [33] N. Isei, M. Sato, S. Ishida S, et al, 1995, Rev. Sci. Instrum. **66** (1), 413
- [34] Y.N. Dnestrovskii and D. P. Kostomarov, "Numerical Simulation of Plasmas", Springer-Verlag, 1986, p. 233.
- [35] V. V. Parail and G. V. Pereverzev, Sov. J. Plasma Phys.,1980, **6**(1), p. 14
- [36]* N.L. Vasin, E. P. Gorbunov, S. V. Neudatchin and G. V. Pereverzev, 1982, Sov. J. Plasma Phys., **8**(2), p. 133
- [37] K.A. Razumova, V. V. Alikaev, A. Y. Kislov et al. Proc. 26th EPS Conf. on Control. Fusion and Plasma Phys. (Maastricht, 1999) ECA vol. 23J (1999) p. 77
- [38]* A. A. Bagdasarov, N. L. Vasin, S. V. Neudatchin and P. V. Savrukhnin, in Proc. of ECE and ECRH Joint Workshop (Hefei, 1989) p. 67
- [39] Y. Kamada, R. Yoshino, M. Nagami, et al, in Plasma Phys. and Control. Nuclear Fusion Research (Proc. 15th Int. Conf., Washington, 1990), vol. 1, IAEA, Vienna (1991) p. 291
- [40] P. Mantica, G. Gorini, G. M. D. Hogeweij, et al., Proc. 26th EPS Conf. on Controlled Fusion and Plasma Physics (Maastricht, 1999) ECA vol. 23J (1999) p. 1109

* Authors are ranged in Russian alphabetical order

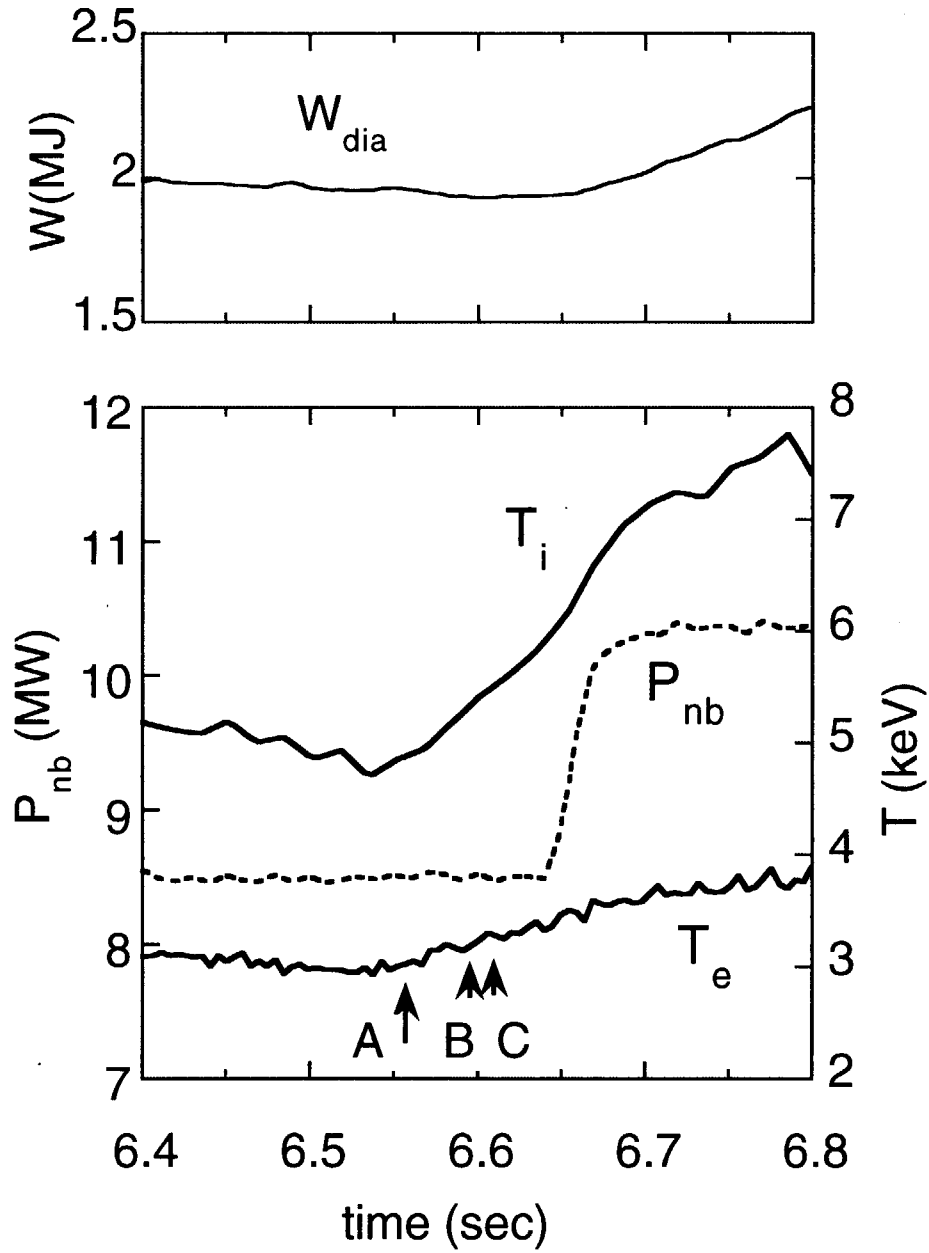


Fig. 1 Evolutions of W_{dia} , P_{NB} , T_i and T_e for an RS discharge E32423. Temperatures are measured near $\rho = 0.45$. Arrows A, B and C indicates the events interested in.

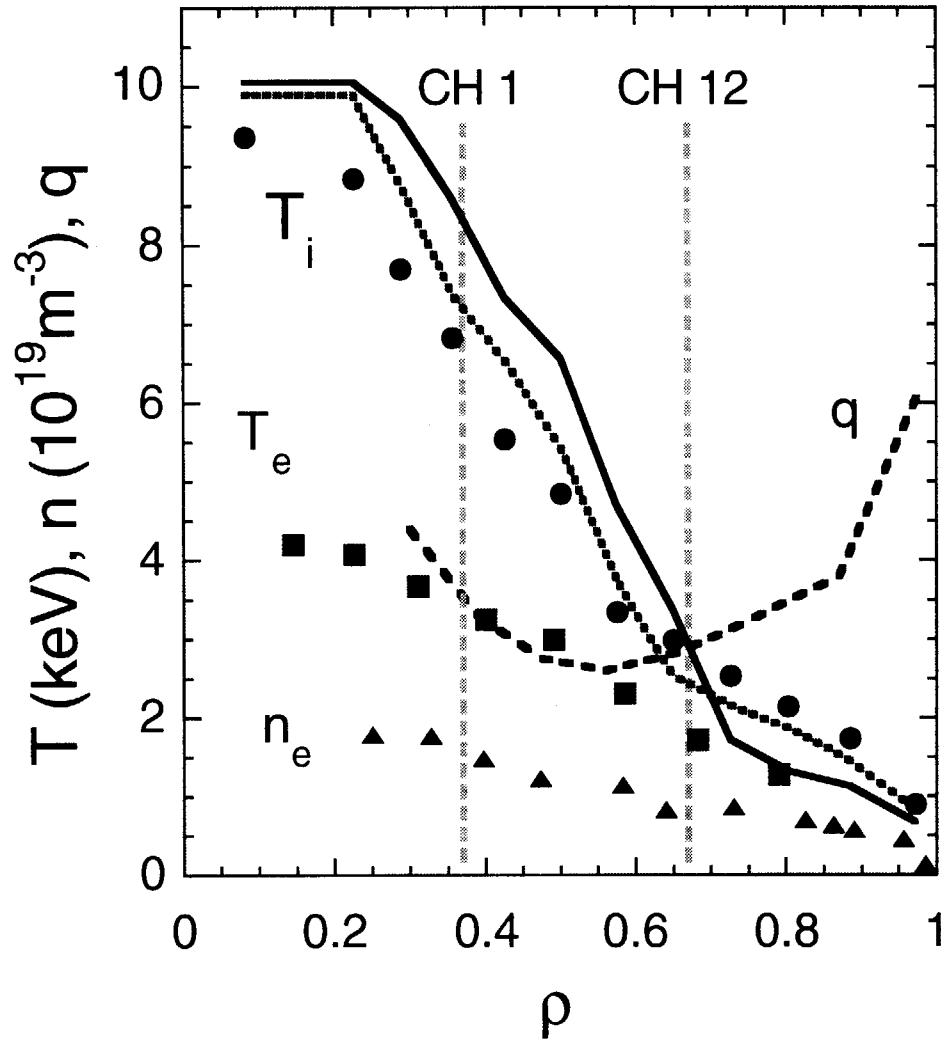


Fig. 2 Radial profiles of T_i (circles), T_e (squares) and n_e (triangles) just before event A at $t=6.560\text{s}$. Fast time-scale evolution of T_e is measured by ECE heterodyne radiometer with 12 channels inside the region $0.37 \leq \rho \leq 0.66$ between two vertical dashed lines. Profiles of T_i for $t=6.604\text{s}$ at event C (dashed line), for $t=6.67\text{s}$ (solid line) and q (dotted line) for $t=6.72\text{s}$ are also shown.

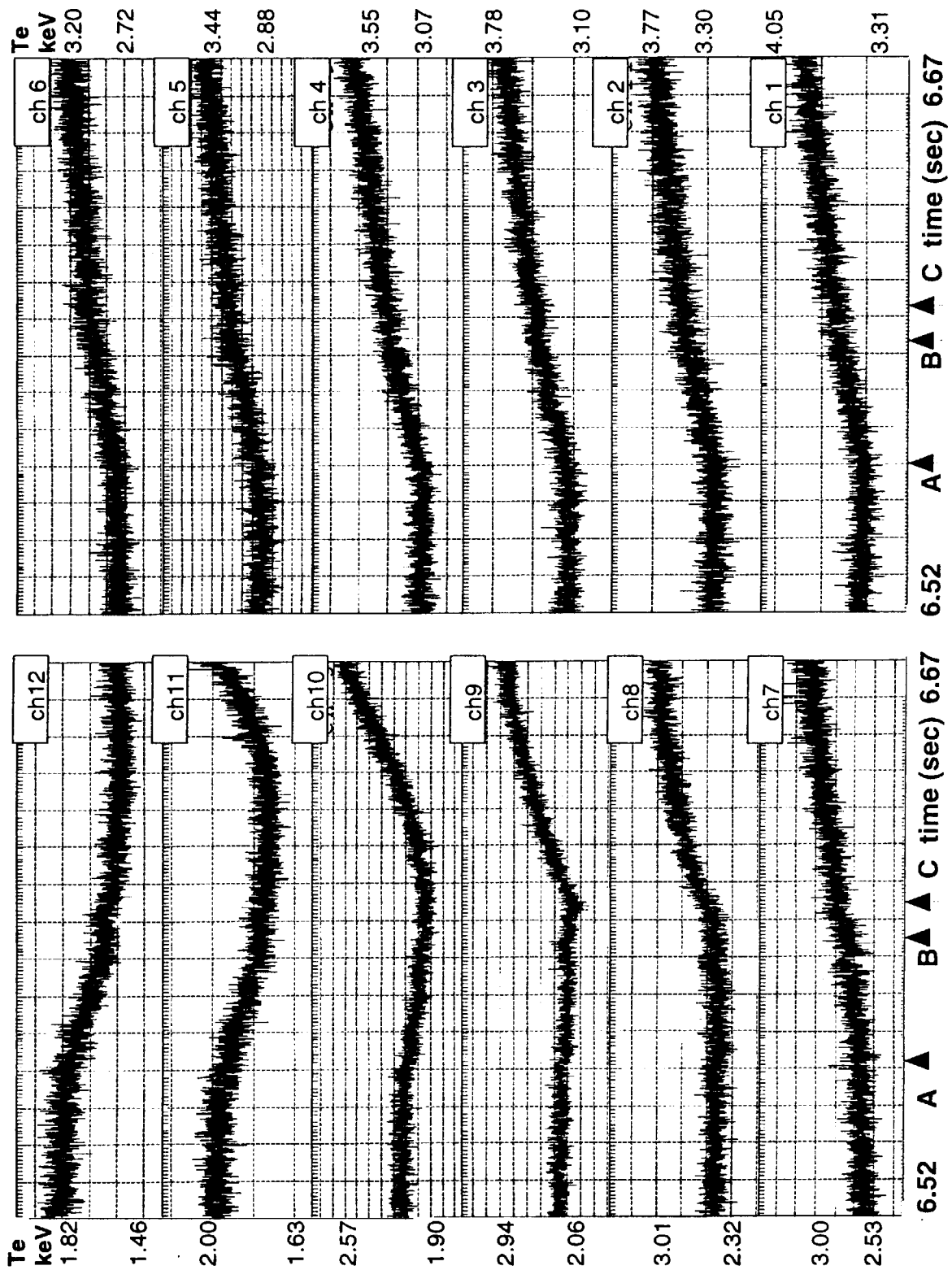


Fig. 3 Te evolution measured on 12 channels of radiometer

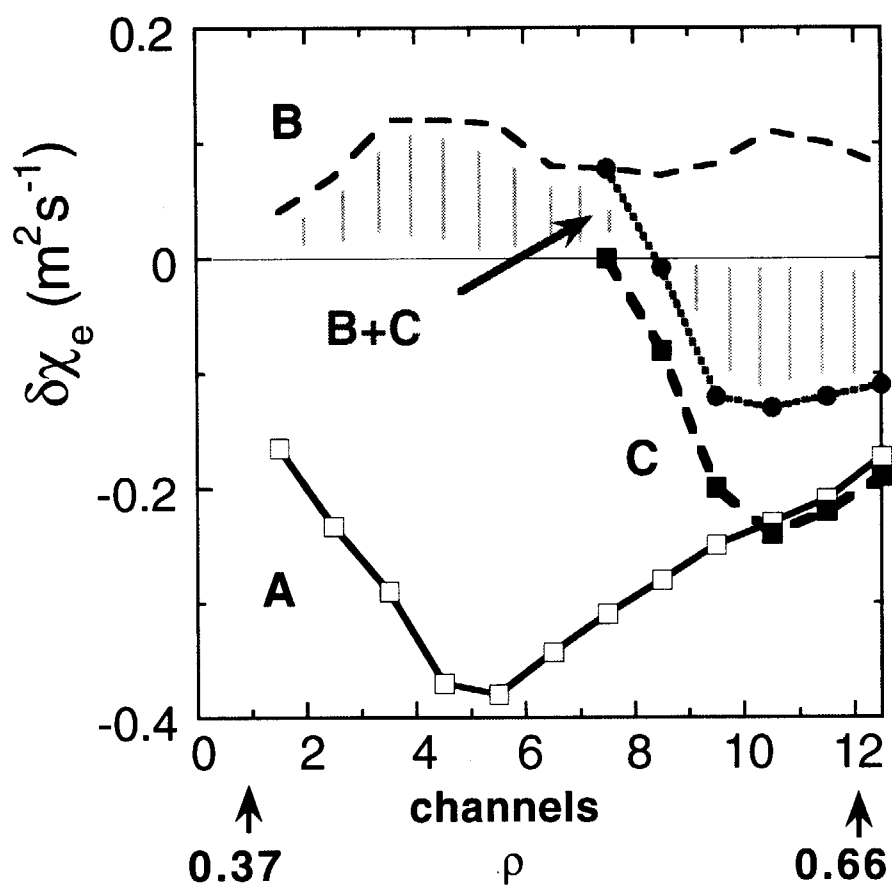


Fig. 4 Profiles of $\delta\chi_e$ for event A(solid line and open squares), for event B (dotted line), for event C (dotted line and solid squares), for sum of events B+C (shadowed region and solid circles).

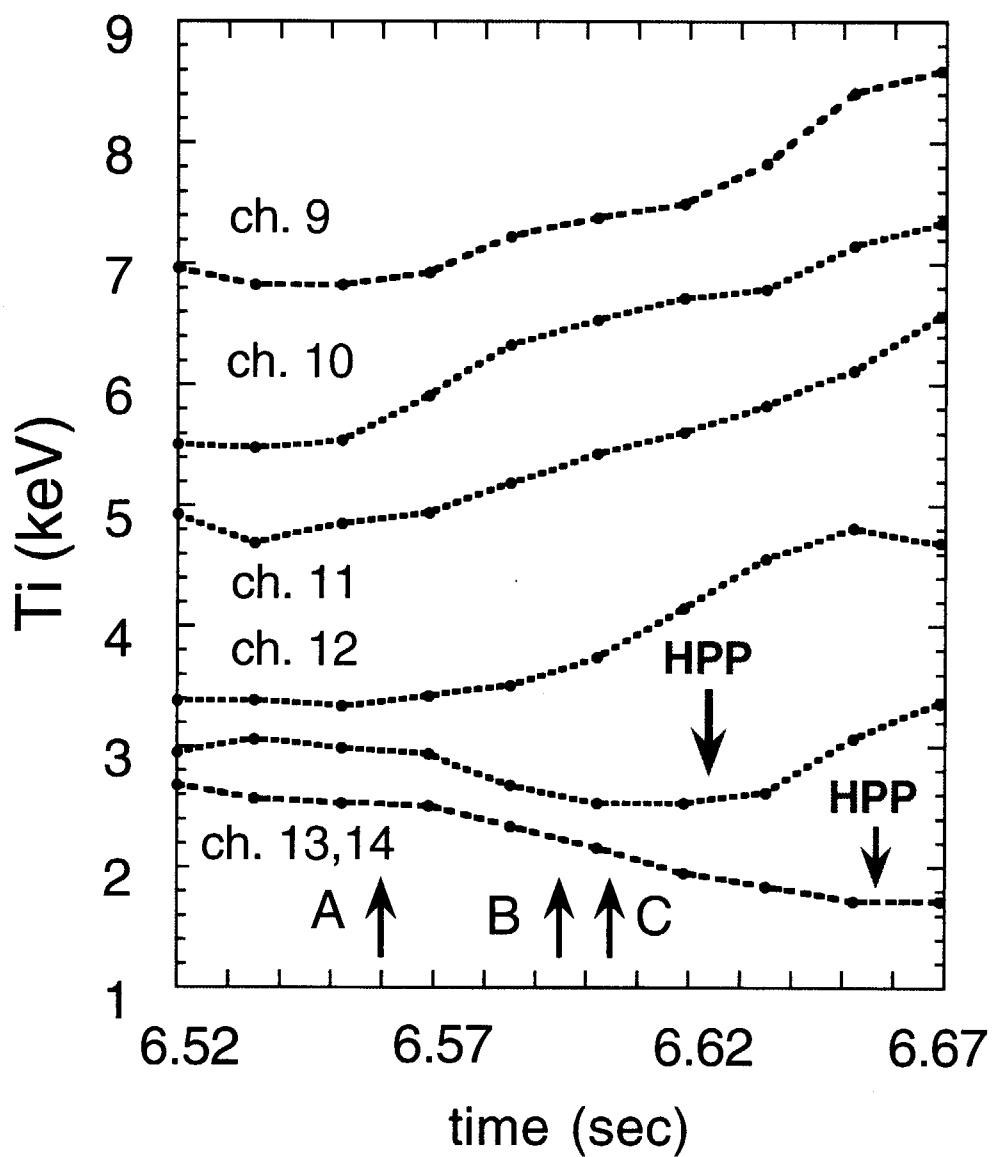


Fig. 5 Time evolution of T_i measured at $\rho=0.36$ (ch. 9), $\rho=0.43$ (ch. 10), $\rho=0.51$ (ch. 11), $\rho=0.58$ (ch. 12), $\rho=0.66$ (ch. 13), $\rho=0.73$ (ch. 14). Events A,B,C are labeled by arrows, region of HPP is marked by HPP arrows.

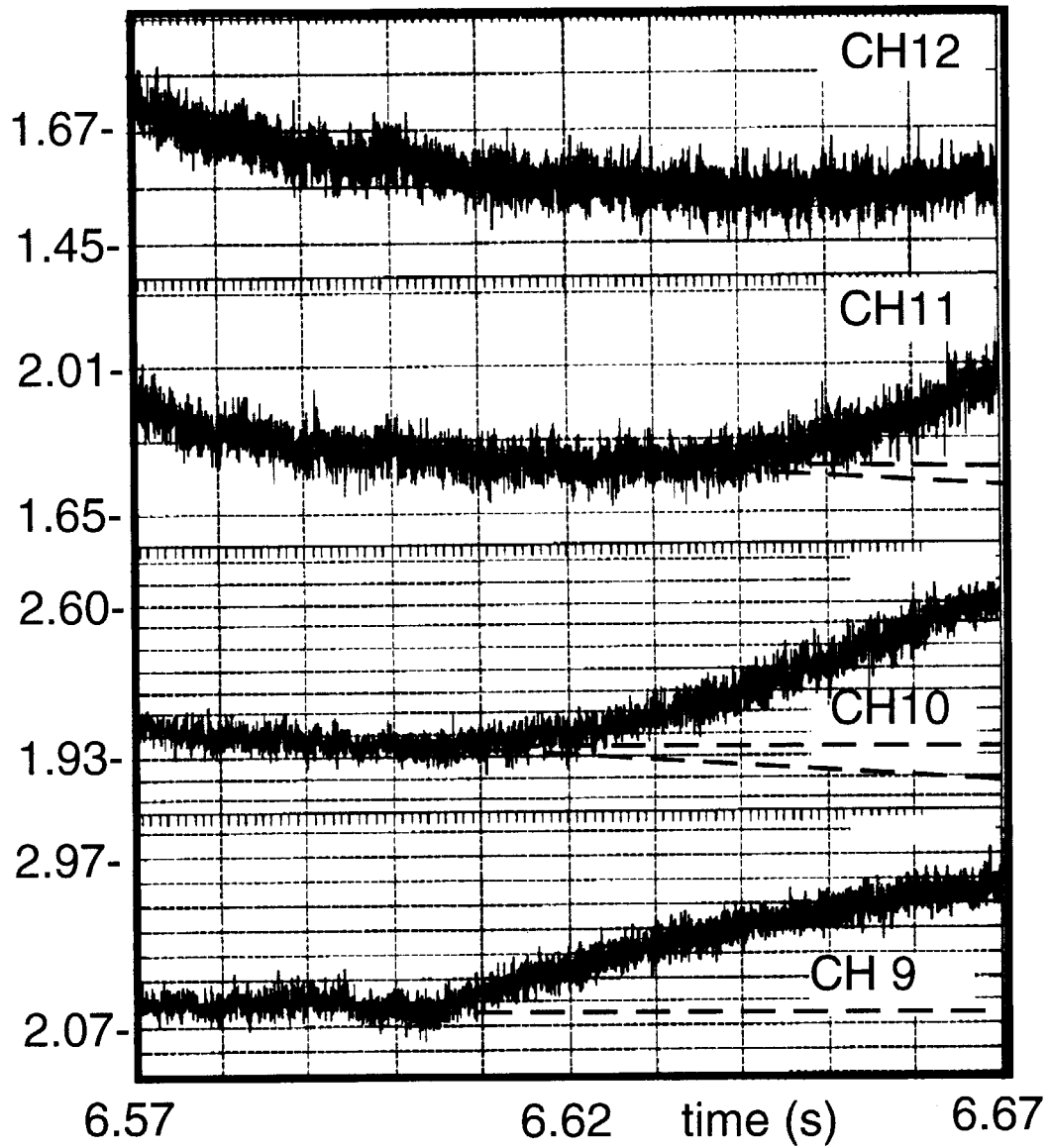


Fig. 6 Evolution of T_e , methods of background subtraction are shown by dotted lines.

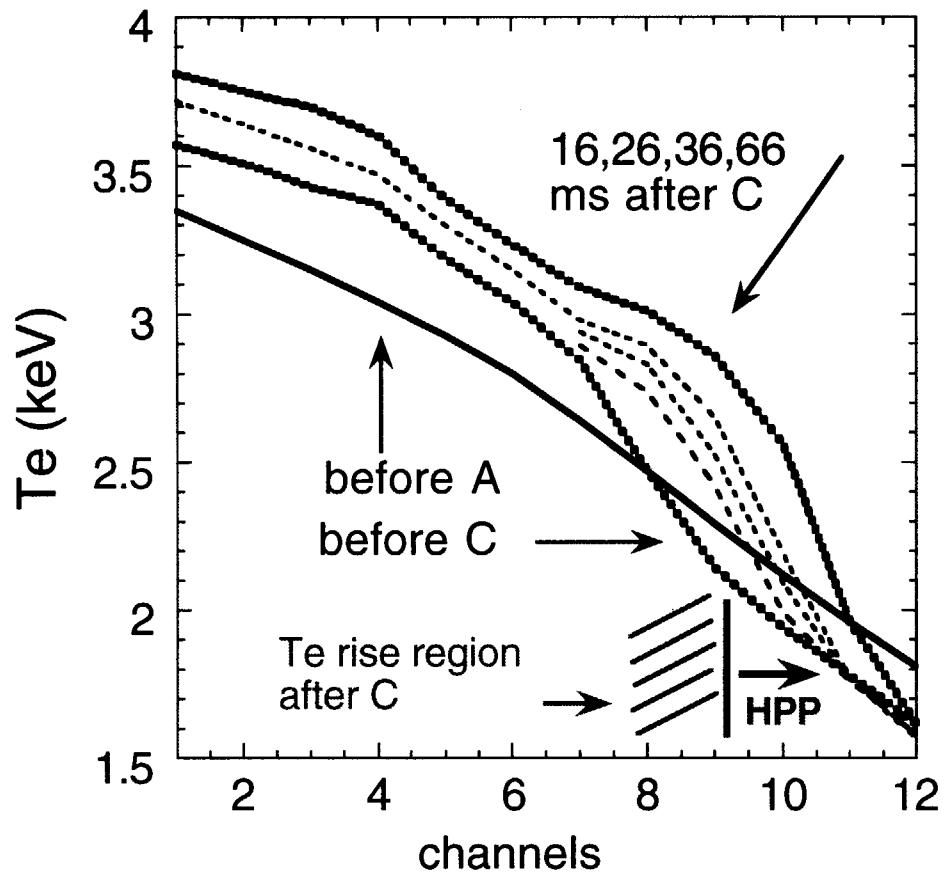


Fig. 7 Profiles of T_e : before event A (solid line); before event C (dashed line); 16,26,36 ms after event C (dotted lines) and 66 ms after event C (dashed line). Region of T_e initial strong rise (source of HPP) is shadowed.

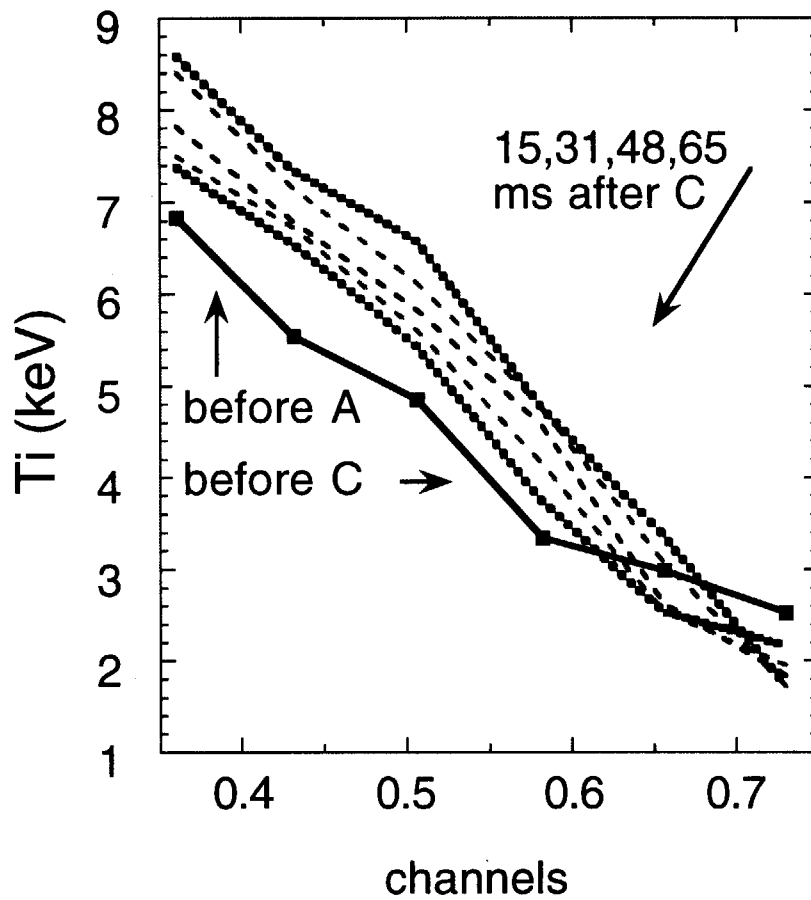


Fig. 8 Profiles of T_i : before event A (solid line); before event C (dashed line); 15,31,48 ms after event C (dotted lines) and 65 ms after event C (dashed line).

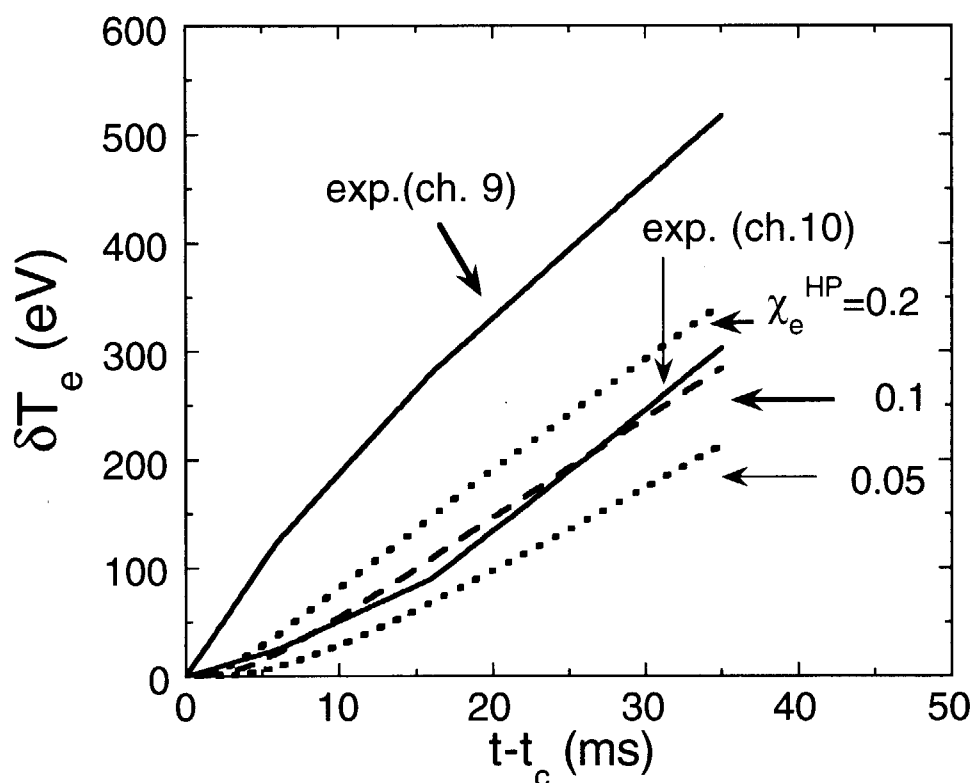


Fig. 9 Electron HPP from ch.9 to ch. 10. Comparison of the experimental δT_e (ch.10,t) (solid line) and calculated δT_e (ch.10,t) with $\chi_e^{\text{HP}} = 0.1 \text{ m}^2/\text{s}$ (dotted line) , with $\chi_e^{\text{HP}} = 0.2$ and $0.05 \text{ m}^2/\text{s}$ (dashed lines). Experimental δT_e (ch.9,t) is the boundary condition for calculations and is shown by solid line.

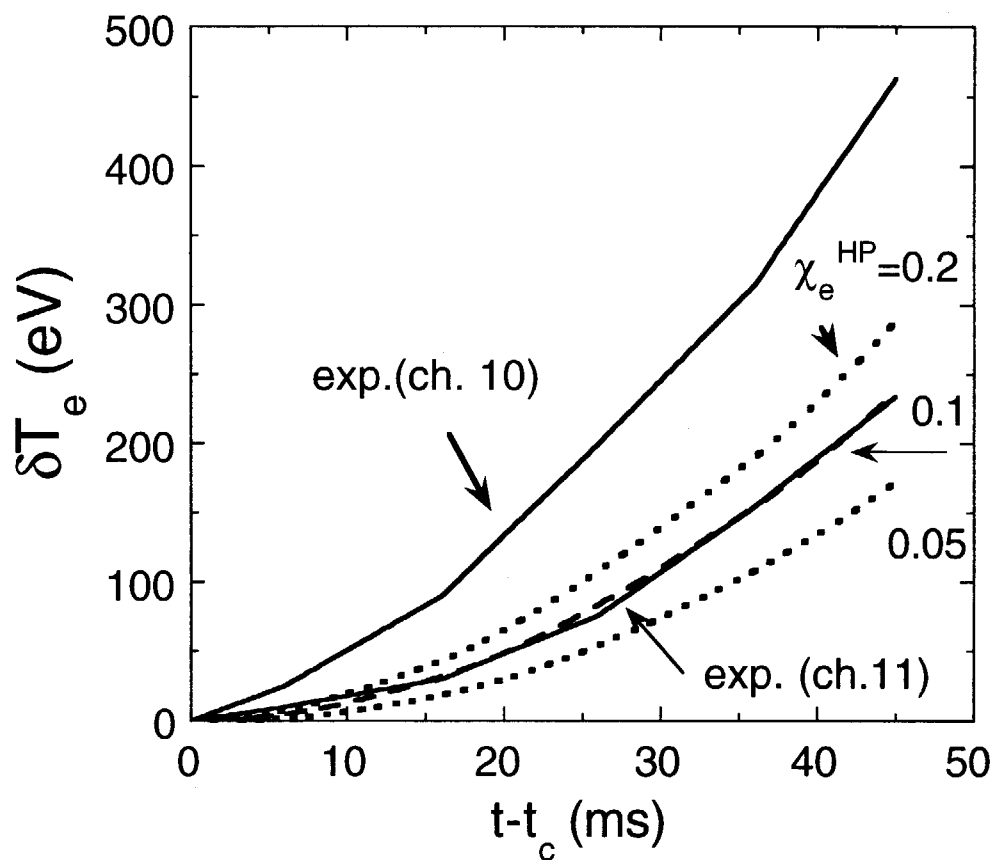


Fig. 10 Electron HPP from ch. 10 to ch.11. Comparison of the experimental δT_e (ch.11, t) (solid line) and calculated δT_e (ch.11,t) with $\chi_e^{HP} = 0.1$ m²/s (dotted line) , with $\chi_e^{HP} = 0.2$ and 0.05 m²/s (dashed lines). Experimental δT_e (ch.10,t) is the boundary condition for calculations and is shown by solid line.

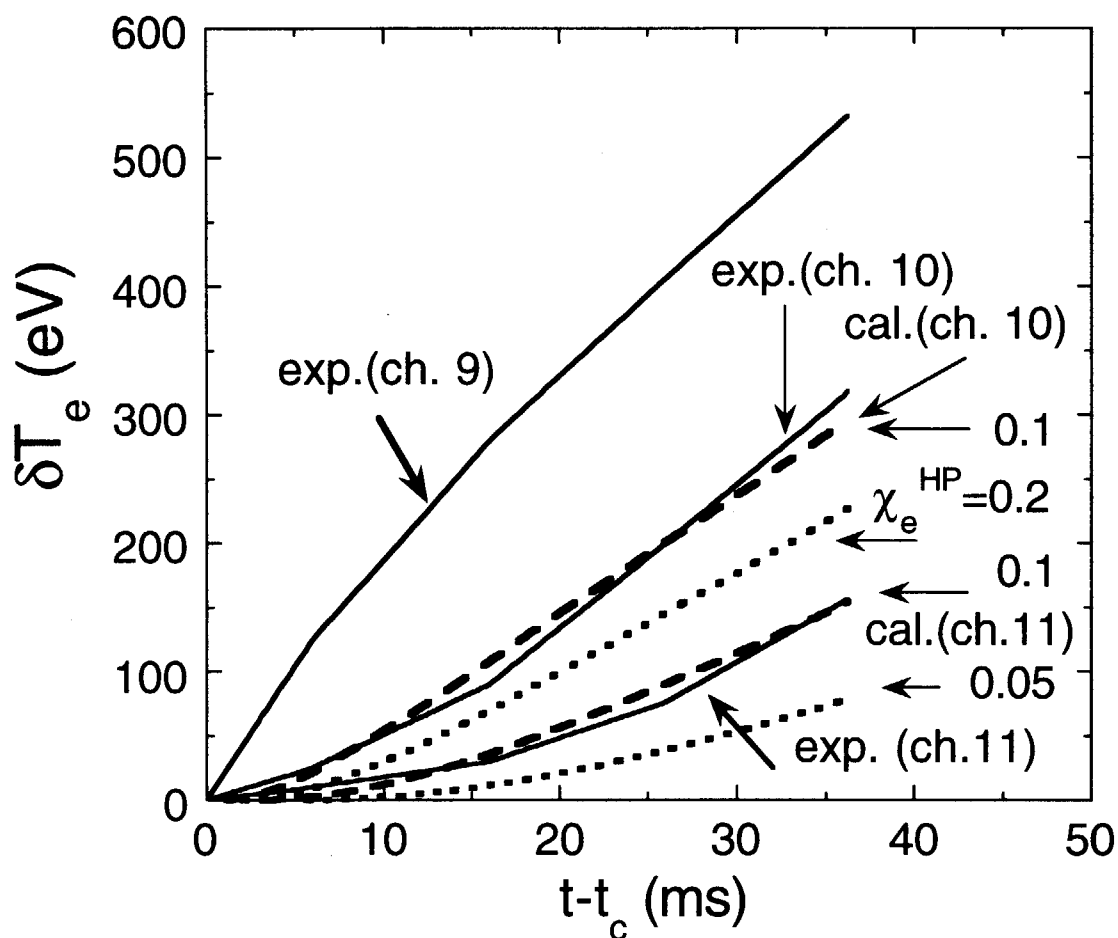


Fig. 11 Electron HPP from ch. 9 to ch. 11. Comparison of the experimental $\delta T_e(\text{ch.11}, t)$ (solid line) and calculated $\delta T_e(\text{ch.11}, t)$ with $\chi_e^{\text{HP}} = 0.1 \text{ m}^2/\text{s}$ (dotted line), with $\chi_e^{\text{HP}} = 0.2$ and $0.05 \text{ m}^2/\text{s}$ (dashed lines). Experimental $\delta T_e(\text{ch.9}, t)$ is the boundary condition for calculations and is shown by solid line. For intermediate zone experimental $\delta T_e(\text{ch.10}, t)$ is shown by solid line and calculated $\delta T_e(\text{ch.10}, t)$ with $\chi_e^{\text{HP}} = 0.1 \text{ m}^2/\text{s}$ is drawn by dotted line.

国際単位系 (SI) と換算表

表1 SI基本単位および補助単位

量	名 称	記 号
長さ	メートル	m
質量	キログラム	kg
時間	秒	s
電流	アンペア	A
熱力学温度	ケルビン	K
物質の量	モル	mol
光度	カンデラ	cd
平面角	ラジアン	rad
立体角	ステラジアン	sr

表3 固有の名称をもつSI組立単位

量	名 称	記号	他のSI単位 による表現
周波数	ヘルツ	Hz	s^{-1}
力	ニュートン	N	$m \cdot kg / s^2$
圧力, 応力	パスカル	Pa	N / m^2
エネルギー, 仕事, 熱量	ジュール	J	$N \cdot m$
工率, 放射束	ワット	W	J / s
電気量, 電荷	クーロン	C	$A \cdot s$
電位, 電圧, 起電力	ボルト	V	W / A
静電容量	ファラド	F	C / V
電気抵抗	オーム	Ω	V / A
コンダクタンス	ジーメンズ	S	A / V
磁束	ウェーバ	Wb	$V \cdot s$
磁束密度	テスラ	T	Wb / m^2
インダクタンス	ヘンリー	H	Wb / A
セルシウス温度	セルシウス度	$^{\circ}C$	
光度	ルーメン	lm	$cd \cdot sr$
照射度	ルクス	lx	lm / m^2
放射能	ベクレル	Bq	s^{-1}
吸収線量	グレイ	Gy	J / kg
線量等量	シーベルト	Sv	J / kg

表2 SIと併用される単位

名 称	記 号
分, 時, 日	min, h, d
度, 分, 秒	$^{\circ}, ', ''$
リットル	l, L
トン	t
電子ボルト	eV
原子質量単位	u

$$1 \text{ eV} = 1.60218 \times 10^{-19} \text{ J}$$

$$1 \text{ u} = 1.66054 \times 10^{-27} \text{ kg}$$

表4 SIと共に暫定的に維持される単位

名 称	記 号
オングストローム	\AA
バーン	b
バール	bar
ガリ	Gal
キュリー	Ci
レントゲン	R
ラド	rad
レム	rem

$$1 \text{ \AA} = 0.1 \text{ nm} = 10^{-10} \text{ m}$$

$$1 \text{ b} = 100 \text{ fm}^2 = 10^{-28} \text{ m}^2$$

$$1 \text{ bar} = 0.1 \text{ MPa} = 10^5 \text{ Pa}$$

$$1 \text{ Gal} = 1 \text{ cm/s}^2 = 10^{-2} \text{ m/s}^2$$

$$1 \text{ Ci} = 3.7 \times 10^{10} \text{ Bq}$$

$$1 \text{ R} = 2.58 \times 10^{-4} \text{ C/kg}$$

$$1 \text{ rad} = 1 \text{ cGy} = 10^{-2} \text{ Gy}$$

$$1 \text{ rem} = 1 \text{ cSv} = 10^{-2} \text{ Sv}$$

表5 SI接頭語

倍数	接頭語	記 号
10^{18}	エクサ	E
10^{15}	ペタ	P
10^{12}	テラ	T
10^9	ギガ	G
10^6	メガ	M
10^3	キロ	k
10^2	ヘクト	h
10^1	デカ	da
10^{-1}	デシ	d
10^{-2}	センチ	c
10^{-3}	ミリ	m
10^{-6}	マイクロ	μ
10^{-9}	ナノ	n
10^{-12}	ピコ	p
10^{-15}	フェムト	f
10^{-18}	アト	a

(注)

- 表1～5は「国際単位系」第5版、国際度量衡局1985年刊行による。ただし、1 eV および 1 u の値はCODATAの1986年推奨値によった。
- 表4には海里、ノット、アール、ヘクタールも含まれているが日常の単位なのでここでは省略した。
- bar は、JISでは流体の圧力を表わす場合に限り表2のカテゴリーに分類されている。
- E C閣僚理事会指令では bar, barn および「血圧の単位」mmHgを表2のカテゴリーに入れている。

換 算 表

力	N (=10 ⁵ dyn)	kgf	lbf
	1	0.101972	0.224809
	9.80665	1	2.20462
	4.44822	0.453592	1

$$\text{粘 度 } 1 \text{ Pa} \cdot \text{s} (N \cdot \text{s} / m^2) = 10 \text{ P (ポアズ)} (g / (cm \cdot s))$$

$$\text{動粘度 } 1 m^2 / s = 10^4 \text{ St (ストークス)} (cm^2 / s)$$

圧	MPa (=10 bar)	kgf/cm ²	atm	mmHg (Torr)	lbf/in ² (psi)
	1	10.1972	9.86923	7.50062×10^3	145.038
力	0.0980665	1	0.967841	735.559	14.2233
	0.101325	1.03323	1	760	14.6959
	1.33322×10^{-4}	1.35951×10^{-3}	1.31579×10^{-3}	1	1.93368×10^{-2}
	6.89476×10^{-3}	7.03070×10^{-2}	6.80460×10^{-2}	51.7149	1

エネルギー・仕事・熱量	J (=10 ⁷ erg)	kgf·m	kW·h	cal (計量法)	Btu	ft·lbf	eV
	1	0.101972	2.77778×10^{-7}	0.238889	9.47813×10^{-4}	0.737562	6.24150×10^{18}
	9.80665	1	2.72407×10^{-6}	2.34270	9.29487×10^{-3}	7.23301	6.12082×10^{19}
	3.6×10^6	3.67098×10^5	1	8.59999×10^5	3412.13	2.65522×10^6	2.24694×10^{25}
	4.18605	0.426858	1.16279×10^{-6}	1	3.96759×10^{-3}	3.08747	2.61272×10^{19}
	1055.06	107.586	2.93072×10^{-4}	252.042	1	778.172	6.58515×10^{21}
	1.35582	0.138255	3.76616×10^{-7}	0.323890	1.28506×10^{-3}	1	8.46233×10^{18}
	1.60218×10^{19}	1.63377×10^{20}	4.45050×10^{20}	3.82743×10^{20}	1.51857×10^{22}	1.18171×10^{19}	1

$$1 \text{ cal} = 4.18605 \text{ J (計量法)}$$

$$= 4.184 \text{ J (熱化学)}$$

$$= 4.1855 \text{ J (15 } ^{\circ}C)$$

$$= 4.1868 \text{ J (国際蒸気表)}$$

$$\text{仕事率 } 1 \text{ PS (仏馬力)}$$

$$= 75 \text{ kgf} \cdot \text{m/s}$$

$$= 735.499 \text{ W}$$

放射能	Bq	Ci
	1	2.70270×10^{11}
	3.7×10^{10}	1

吸収線量	Gy	rad
	1	100
	0.01	1

照射線量	C/kg	R
	1	3876
	2.58×10^{-4}	1

線量当量	Sv	rem
	1	100
	0.01	1

(86年12月26日現在)

ANALYSIS OF INTERNAL TRANSPORT BARRIER HEAT DIFFUSIVITY FROM HEAT PULSE PROPAGATION CREATED BY ABRUPT VARIATION OF DIFFUSIVITY IN JT-60U REVERSE SHEAR PLASMAS